Ocean Systems Engineering, *Vol. 16, No. 1 (2026) 33-62*
https://doi.org/10.12989/ose.2026.16.1.033

Techno-Press

Seakeeping-performance comparisons of monohull, catamaran, and SWATH crew-transfer vessels in operational-limit sea states

Muhammad Zaid bin Zainuddin[1], MooHyun Kim*[1], Krish T. Sharman[2], Suqin Wang[3]

[1] *Department of Ocean Engineering, Texas A&M University, College Station, USA*
[2]*Department of Mechanical and Industrial Engineering, University of Massachusetts Amherst, USA*
[3]*ABS (American Bureau of Shipping), Houston, USA*

(Received November 12, 2025, Revised February 22, 2026, Accepted March 2, 2026)

Abstract. Three different hull forms, monohull, catamaran, and SWATH (small waterplane area twin hull), of similar displacement and principal dimensions are designed for the systematic comparisons of their seakeeping performances in sea state 3 and 4, which is considered as the typical operational limit of CTVs (crew transfer vessels). The RAOs (response amplitude operators) of the three vessels for various wave headings were calculated from potential theory and BEM (boundary element method) in the frequency domain. In parallel, the time-domain simulations including viscous drag effects were also conducted for their motions in sea state 3 and 4 by using an independent in-house program, CHARM3D, which compared well against the frequency-domain results. When comparing seakeeping performance in sea state 3 and 4, the SWATH vessel outperforms both the catamaran and the monohull. The SWATH's 6DOF motion amplitudes are about half of those of catamaran and monohull since its heave-roll-pitch natural frequencies are much lower than the peak frequencies of incident waves in sea state 3 and 4. Therefore, we found that a SWATH can be operated up to a higher sea state 4 while a monohull and a catamaran can be used up to sea state 3. Our simulations also examined the three CTVs positioned about 10 m behind a monopile wind turbine structure of 10 m-diameter, by using our in-house two-body CHARM3D hydrodynamic interaction simulation programs. The two-body simulation results show minor shield effects in motions when operating behind the monopile. Again, SWATH shows the best seakeeping performance compared to other vessels.

Keywords: catamaran; monohull; motion comparison; operational limit; seakeeping performance; SWATH; two-body interaction

1. Introduction

The offshore wind-energy industry is one of the fastest growing sector among various ocean renewable energy businesses. Recent trend shows that there will be more floating wind farms in deeper waters than fixed ones in shallow waters in the coming years due to easier government permission and less resident opposition. For maintenance, repairs, and inspections of those offshore wind turbines, skilled crew members need to be dispatched and their safety as well as CTV (crew transfer vessel) efficiency is an important operational issue [1]. In this regard, this paper focuses on the performances of 3 different types of CTVs [2], monohull, catamaran, and SWATH (small

*Corresponding author, Professor, E-mail: m-kim3@tamu.edu

http://www.techno-press.org/ose/5
ISSN: 2093-6702 (Print), 2093-677X (Online)

waterplane area twin hull) of similar displacement and principal dimensions, in potentially maximum dispatchable sea states i.e., sea state 3 or 4. Otsubo et al. [3-5] investigated the feasibility of jump-on land from three CTVs by applying bow-fender friction to reduce pertinent relative motions. In another paper, crew transfer through walk-to-work (W2W) gangway [6] connecting CTVs to 15 MW monopile is investigated. The safety of the operation is checked by both frequency-domain RAOs and time-domain simulations. Gutsch et al. [7] validated relative motion RAO approach for simulating W2W gangway operations between service vessel and floating turbine, which found that floater-to-floater operations typically experience greater gangway motions than floater-to-fixture connections, particularly in short-period waves, while wave-interaction effects remain minor when only first-order wave forces are considered.

CTVs can be broadly classified based on their hull geometry (e.g., Thiagarajan [2]). Catamarans have two long demi hulls that are connected by a common deck structure. The spacing of the demi hulls can be altered to accommodate space requirements, which also influences roll stability in waves. Specific features of a catamaran CTV are (i) popular for crew transfer in offshore wind, (ii) large working space and payload onboard, (iii) motions are relatively high, (iv) typical limiting significant wave heights is 1.5 m, and (v) typical length is about 20's m, speed range between 20 and 25knots.

A SWATH has a small water plane area and is different from a catamaran in underwater hull shape. The small waterline area has some advantages in vessel motion with the penalty of reduced roll stability which can be controlled by the location of COG (center of gravity). Notable features of SWATH CTV are (i) better motion performance compared to catamaran and monohull, (ii) large working space, and (iii) expanded operational window. Its typical length is about 20's m and speed range between 20 and 25 knots.

Monohulls are the traditional form of oceangoing vessels. They are highly available and economical to buy and maintain. Specific features of a monohull CTV are (i) relatively high motions, (ii) limited workable deck area while having extra below-deck storage space, and (iii) operational limit for significant wave height > 1.5 m. Its typical length is in the 20's m range, speed ranging from 20 and 25knots.

Among the hull forms analyzed, monohulls performed the worst in terms of heave motion and roll stability, an essential factor for safe crew transfers. Compared to the monohull shape, catamarans demonstrated slightly better heave motion and significantly better roll stability. SWATH showed excellent performance in both heave and roll, though their roll stability may highly depend on vessel loading and location of center of gravity. Monohulls and catamarans are simpler to design and construct while SWATHs are more complex to design and build due to much less data base and operational experience. H_S 1.5 m and 2.5 m are typical sea conditions corresponding to states 3 and 4. If a particular vessel is operable even in sea state 4, its overall operational window will significantly be expanded. In this regard, SWATH has advantage over the other two vessels despite its unpopularity in currently available fleets.

Based on the above experience-based information, three typical generic service vessels of similar length and displacement, monohull, catamaran, and SWATH, are designed to represent the respective vessels' main characteristics. The adopted hull geometries are very simple for easier fabrication and not necessarily optimal design in terms of seakeeping performance. In this paper, only the hull geometries below MWL (mean water level) are used to compare their hydrodynamic/seakeeping performances in the same wave conditions without specifying the details of superstructures above MWL. Then, 3D BEM (boundary element method) is applied i.e., their wetted hull geometries below MWL are discretized by numerous constant quadrilateral

Table 1. Principal characteristics of the 3 vessels

	Wet volume (m^3)	Length (m)	Width (m)	Draft (m)	VCG (m)	VCB (m)	Waterplane Area (m^2)
Monohull	177	26.5	6.8	1.3	-0.3	-0.58	156.65
SWATH	197	26.5	7.5	3	-0.9	-2.1	26.50
Catamaran	161	26.5	8	2	-0.3	-1	81.00

panels to solve for the vessels' hydrodynamics and motion/seakeeping capabilities in regular and irregular waves. For this, the 3D diffraction/radiation BIEM (boundary integral equation method) commercial program WAMIT [8] calculated requisite hydrodynamic coefficients and 2nd-author's in-house program CHARM3D [9] was subsequently used for the ensuing time-domain simulations in the applied random waves of sea state 3 and 4. Morison members were also employed in the time-domain simulations to represent additional viscous drag forces particularly in the case of SWATH and catamaran.

Finally, the motions of the 3 CTVs behind (separation distance=10 m) a 15 MW monopile (diameter=10 m) wind turbine were simulated by using 2-body time-domain-simulation programs to check the safety of gangway crew transfer to observe whether their motions can be increased because of two-body hydrodynamic interactions. It is shown that vessel motions behind the monopile tend to be slightly reduced due to the shield effect although it depends on the shapes of RAOs and incident wave conditions. On the other hand, Barthelemy [10] showed that when close-contact berthing against a smaller 5 m diameter monopile, CTVs are fully exposed to incident waves, leading to increased deck flooding risk.

The present paper is organized in the following way. Sec.2 describes the designs and particulars of the 3 generic CTVs with the descriptions of the applied sea state 3 and 4. Sec.3 compares the potential-theory-based RAOs (response amplitude operators) of the three CTVs for various wave headings. Sec.4 compares the time-domain simulations of the three CTVs in sea state 3 and 4, which leads to the assessment of their relative motion/seakeeping performances. Sec.5 considers two-body hydrodynamic interactions of 10 m-diameter monopile and 3 CTVs to assess potential shield effect and the safety of crew transfer through gangway. Sec.6 summarizes important findings and conclusions.

2. Three generic CTVs

Three simple and representative hull forms of monohull, catamaran, and SWATH with similar displaced volumes and principal dimensions are designed to compare their relative seakeeping performances in the upper limits of sea state 3 and 4, which are summarized in Tables 1 and 2.

Their wet body surfaces at mean positions were discretized by numerous quadrilateral plane panels for subsequent hydrostatic and hydrodynamic calculations based on potential theory and boundary element method, for which a commercial 3D diffraction/radiation panel program WAMIT was used. The isometric views of the three vessels by CAD and with panel discretization are shown below in Fig. 1. A total of 840, 1272, and 2585 panels were used for the discretization of the wetted surfaces of monohull, catamaran, and SWATH, respectively. The coordinate

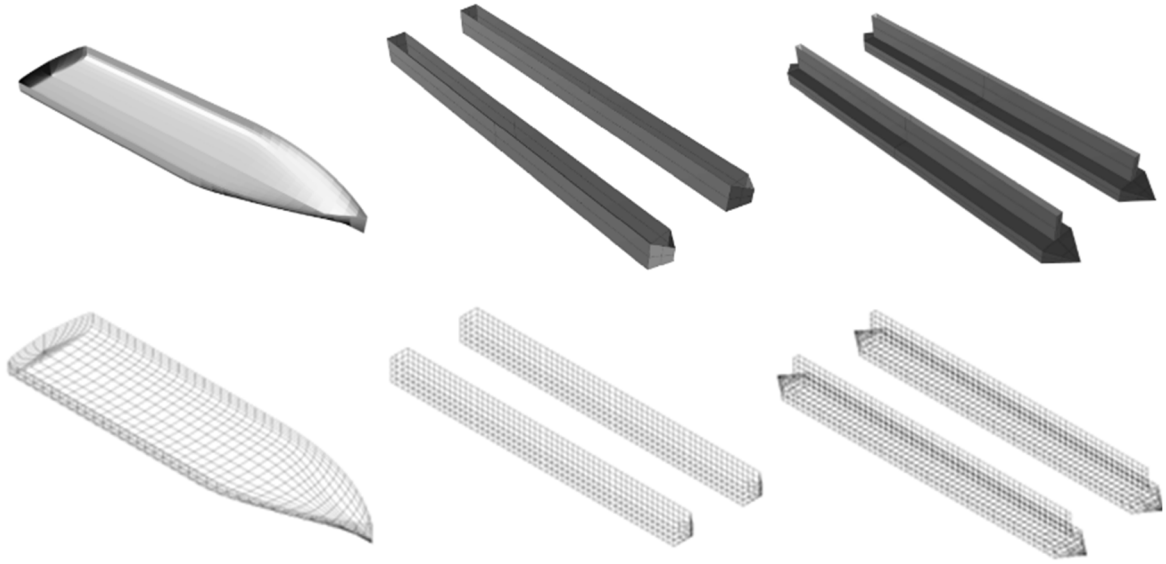

Figure. 1 CAD view of 3 vessels' wetted hull surface below MWL (mean water line) and the corresponding panel-based discretization. From left to right: monohull, catamaran and SWATH

origin in the hydrodynamic calculation is located at MWL above vessel's center of gravity in longitudinal direction (x axis) and vertical axis z positive upward. All the ensuing motion results are presented with respect to the origin of the coordinate system.

To generate the simplistic monohull form, its frontal part is captured from modified Wigley hull form, and the rear part is a straight hull surface of constant width. This shape is very similar to several existing service vessels. A catamaran consists of two thick hulls at both ends of deck width to secure enough displacement for supporting the deck payload. This is the most popular hull types to serve as CTVs. Again, the simple hull shapes are designed to have only straight plates without any curvature. A SWATH is composed of vertical hulls at both ends of width and horizontal-plate pontoons at their bottoms. The major differences of the 3 vessels are in respective waterplane areas, monohull with large waterplane area, catamaran with moderate waterplane area, and SWATH with the smallest water plane area.

In case of CTVs, the weights of hull and deck structures (payloads) are supported by buoyancy proportional to the displaced volume. Therefore, with the similar displaced volume, as in the present comparative study, the seakeeping performance can be determined depending on the shape of hull, especially on the magnitude of waterplane area. The monohull has the advantage of larger storage space inside the hull for cargo but in case of CTV this is not essential. Instead, a wider deck area is preferred, which can be easily obtained by using a catamaran and SWATH. The heave natural frequency (ω_n) of the vessel is given by

$$\omega_n = \sqrt{\frac{A_w}{m+m_{33}}}, \tag{1}$$

where

A_w=waterplane area, m=real mass, and m_{33}=heave added mass.

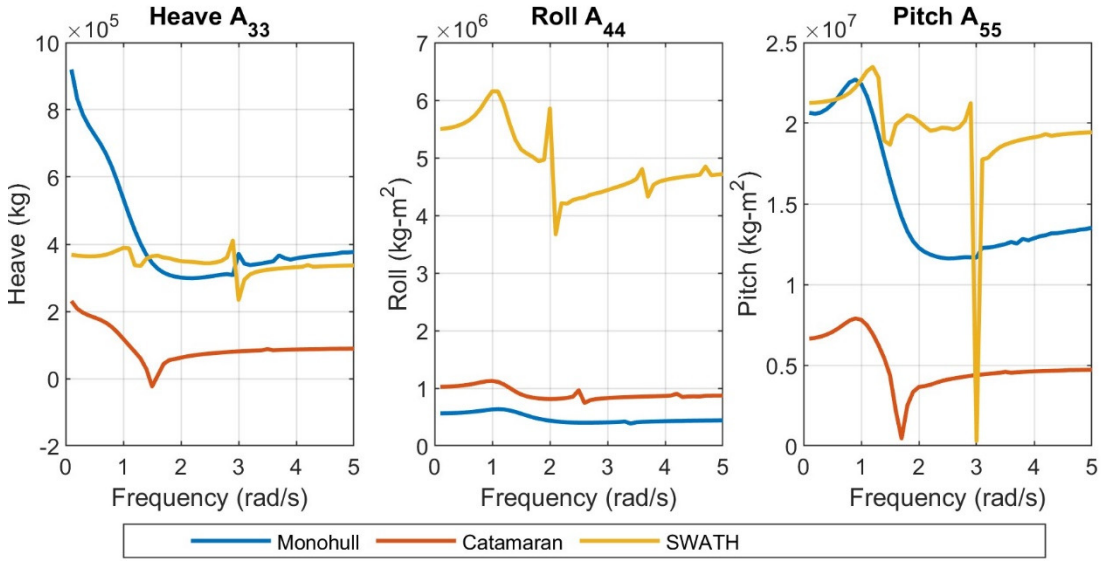

Figure 2. Heave-roll-pitch added mass comparison of the 3 vessels (water depth h=30 m)

In case of the monohull shape of the given size, its heave natural frequency (1.8rad/s) is higher than the spectral peak frequency (ω_p) of sea state 3 and 4, which means that heave motions tend to be similar to wave elevations in the static-control zone. The same is also true for the catamaran. To have smaller heave motions in those sea states, the vessel's heave natural frequency should be much lower than the ω_p of sea state 3 and 4 so that it can fall into the inertia-control zone. One way is to reduce water plane area like in a SWATH. Another way is to further increase heave added mass. In case of catamaran hull, its waterplane area is reduced compared to monohull but heave added mass is also reduced, and thus their effects are compensated so that significant shift of heave natural frequency may not happen. The present design of SWATH has the smallest waterplane area with significantly increased heave added mass due to the pontoon's large flat area, both of which contribute to a significantly lower heave natural frequency. The flat-pontoon area also contributes to significant increases in viscous drag forces in heave, roll, and pitch modes. Conventional SWATH has circular-cross-sectioned pontoons but considering the above benefits, the pontoon shape is designed to have a flat rectangular section. The added mass of the circular-cross-sectioned pontoons can also be very small or negative at certain frequencies [11], which is not favorable for heave performance. In Figs. 2-4, the comparisons of heave-roll-pitch added masses, hydrostatic coefficients, and heave RAOs of the 3 vessels in head wave are given. The added mass and RAO results are based on potential theory. The expected viscous-drag effect in heave-roll-pitch is the largest in SWATH, moderate in catamaran, and small in monohull, which will further be observed in the next section through comparisons with time-domain simulations. The heave-roll-pitch added mass (or moment of inertia) of the SWATH are the largest among the 3 vessels. The large added mass of SWATH is due to the contribution from flat bottom pontoon. There exist sharp variations in the SWATH added mass, which is related to trapped modes between the two hulls. We checked that those are not caused by irregular frequencies by comparing with irregular-frequency-removal option. On the other hand, SWATH's heave-roll-pitch restoring coefficients are the smallest due to

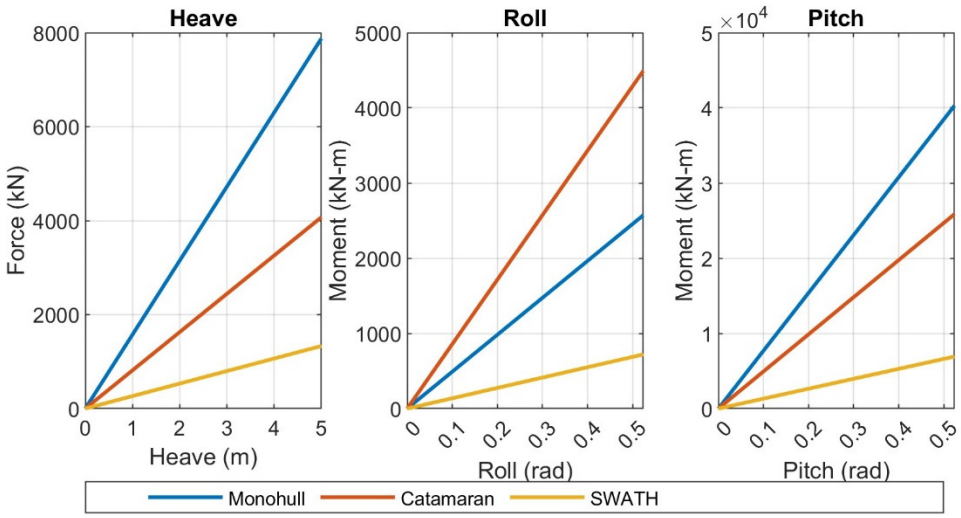

Figure 3. Heave-roll-pitch linear hydrostatic restoring coefficients of the 3 vessels

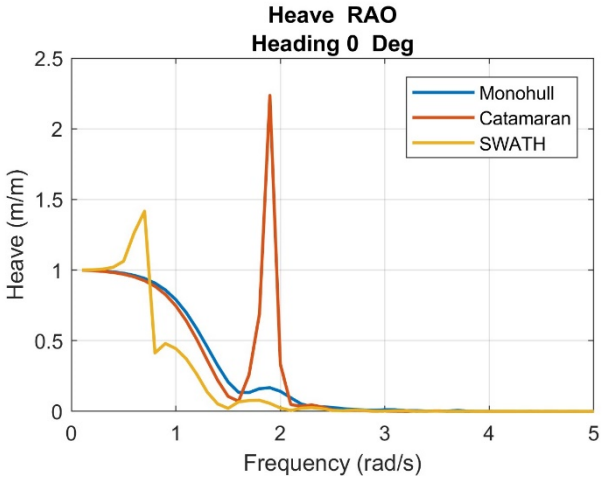

Figure 4. Heave RAO comparisons in head wave for the 3 vessels (water depth $h = 30\ m$)

its smallest waterplane area. The combined effects of large added mass and reduced hydrostatic stiffness of SWATH locate its natural frequencies far below the peak frequencies of typical operational-limit of sea state 3 and 4 (see Fig. 4).

The intact transverse (roll) stability of a freely floating vessel can be estimated from submerged weight ($V\rho g$) times GM where V is displaced volume, ρ is sea-water density, g is gravitational acceleration, and GM is metacentric height. The GM can be calculated from $GM = KB + BM - KG$, where KB is distance from the keel (hull bottom) to the center of buoyancy (centroid of displaced mass), KG is distance from the keel to the body-mass center, and $BM = \frac{I_{xx}}{V}$ with I_{xx} = second moment of the waterplane area with respect to the x axis. The linear hydrostatic restoring coefficients of roll, C_{44}, are compared in Fig. 3 among the 3 vessels.

Table 2. Additional information for the 3 CTVs

	Wet vol per mass (m^3/ton)	Center of gravity (x, y, z) (m)	Center of buoyancy (x, y, z) (m)	Roll-pitch-yaw radius of gyration (r_{44}, r_{55}, r_{66}) (m)	Hydrostatic coefficients C_{33}, C_{44}, C_{55} N/m, Nm/rad, Nm/rad
monohull	0.975	(-1.8, 0, -0.3)	(-1.8, 0, -0.58)	2.25, 6.62, 6.62	1.6×10^6 4.9×10^6 7.7×10^7
SWATH	0.975	(0,0,-0.9)	(0,0,-2.1)	3.5, 6.62, 6.62	2.7×10^5 1.4×10^6 1.3×10^7
catamaran	0.979	(0,0,-0.3)	(0,0,-1)	3.5, 6.62, 6.62	8.1×10^5 7.6×10^6 4.8×10^7

The heave RAO comparisons given in Fig. 4 show that the heave RAOs of monohull and catamaran have similar heave natural frequencies around 1.8rad/s, where monohull's resonant peak is much smaller than that of catamaran due to monohull's much larger heave radiation (motion-induced) damping there. On the other hand, the heave natural frequency of SWATH is located near 0.65 rad/s. The typical peak wave periods of sea state 3 and 4 are located in the range of 4~6s (1~1.5 rad/s). It is seen that the heave RAO of SWATH is the smallest in the range.

3. RAO Comparisons of three CTVs

The 6DOF RAOs are calculated by WAMIT for 3 different wave headings (head, 45-deg, and beam waves) and for 3 CTVs operating at a water depth is 30 m. The following additional information used for the motion RAO calculation is given in Table 2. The coordinate origins of the vessels are located at their COG in x-y and z=0 m (MWL) with z axis positive upwards.

3.1 Monohull case

In the monohull case, the heave/roll/pitch natural frequencies are 1.8/1.9/2.0 rad/s (3.49/3.31/3.14 s). There, the potential (radiation) heave-pitch damping is large, so heave-pitch resonance peak is small. In beam sea condition, the heave RAO is greater than 1, i.e., heave amplitude can be larger than wave amplitude in the frequency range of typical sea state of 3 and 4 (1~1.5 rad/s), which is unfavorable in view of sea-keeping performance. The roll resonance peak is significant since the corresponding potential-based roll radiation damping is small, as is typical of a conventional ship hull. A well-known solution to this problem is to add a bilge keel to reduce the roll motion in the operational sea state of 3 and 4, for which appreciable wave energy is present near the natural frequency.

3.2 Catamaran case

The catamaran has two vertical rectangular hulls of thickness 1.5 m and draft 2 m. The heave-roll-pitch natural frequencies of the catamaran vessel are 1.9, 1.7, and 2.1 rad/s. The natural

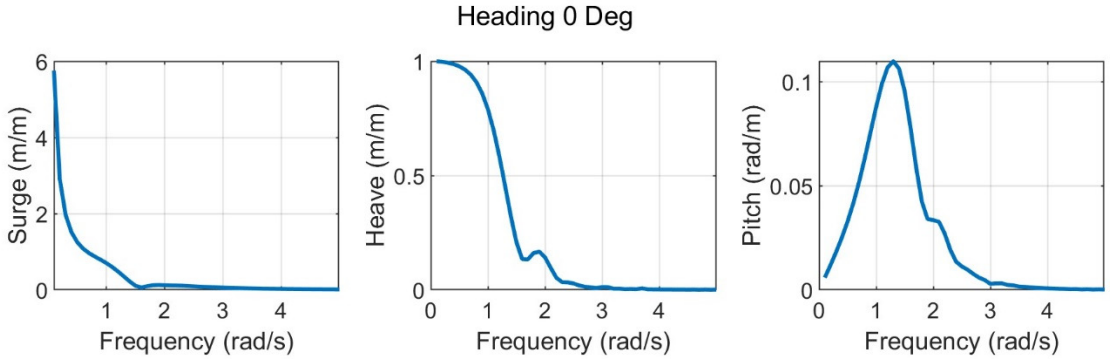

Figure 5. RAOs of monohull in head incident waves

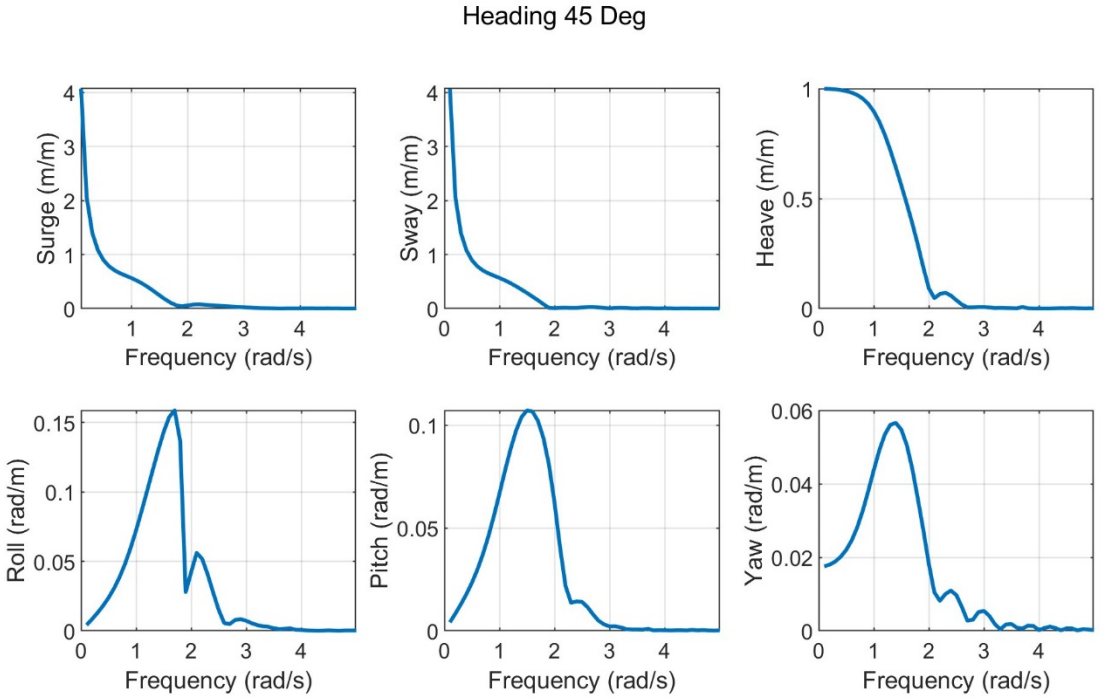

Figure 6. 6-DOF RAOs of monohull in 45deg oblique incident waves

frequency was obtained through eigenvalue analysis of the free-undamped system's equation of motion with added mass taken at the respective natural frequencies. In beam wave, the heave RAO is greater than 1 in the range of 1~1.3 rad/s, which is similar to the monohull case and unfavorable in view of sea-keeping performance in the sea state of 3 and 4. In beam short waves, sharp resonance amplification of heave is observed near its natural frequency, which is due to smaller heave-induced radiation damping compared to the monohull. The roll can also be larger near 1.75 rad/s, which will be reduced after introducing viscous drag force. The roll radiation damping of the

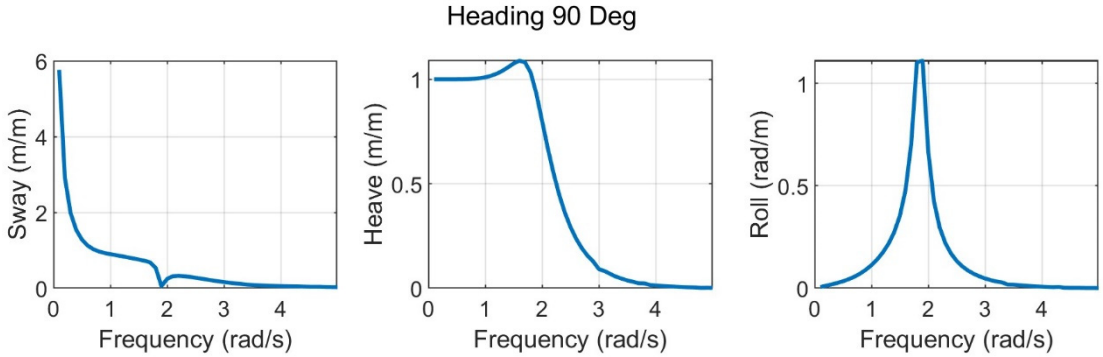

Figure 7. RAOs of monohull in beam incident waves

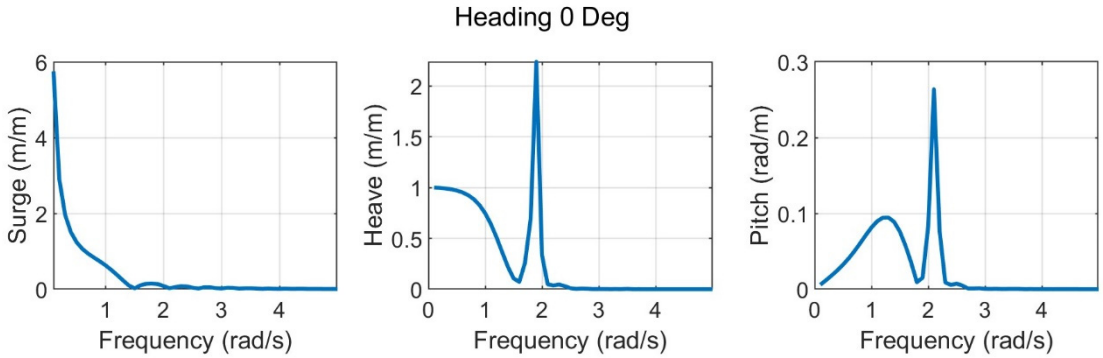

Figure 8. RAOs of catamaran in head incident waves

catamaran is not large since roll-motion-induced radiated waves can be trapped between the two vertical hulls.

3.3 SWATH case

In Figs. 11-13, the heave-pitch motions of SWATH are about half of those of monohull and catamaran. In beam wave, the roll RAO is significantly smaller than those of monohull and catamaran. Those motion amplitudes are to be further reduced by adding significant viscous drag effects. The SWATH's heave-roll-pitch natural frequencies are estimated to be 0.68, 0.42, 0.66 rad/s, which are away from the wave peak frequencies of sea state 3 and 4. In view of RAO comparisons, SWATH's seakeeping performance in sea state 3 and 4 seems much better than those of monohull and catamaran, which means that SWATH can greatly expand its operational window up to upper limit of sea state 4 (e.g., H_s 2.5 m).

From the above results, the rule of thumb is that the heave/roll/pitch of SWATH are less than half of heave/roll/pitch of monohull and catamaran regardless of incident wave angles. This conclusion coincides with the general observation made in wind industry although the number of SWATH vessels is quite small.

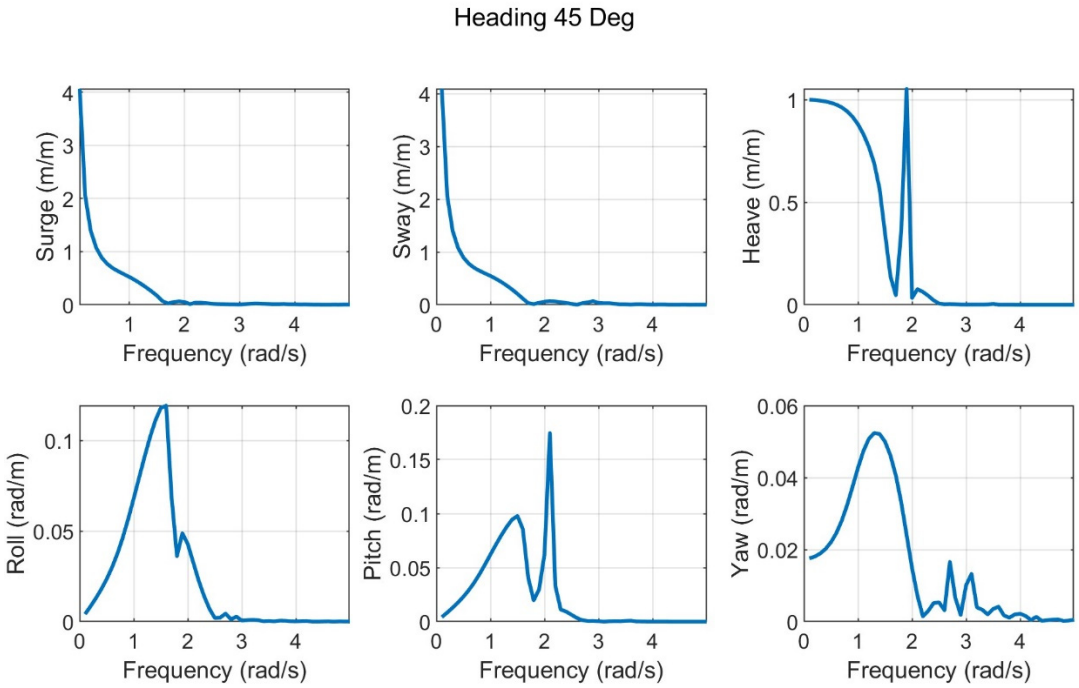

Figure 9. 6DOF RAOs of catamaran in 45deg oblique incident waves

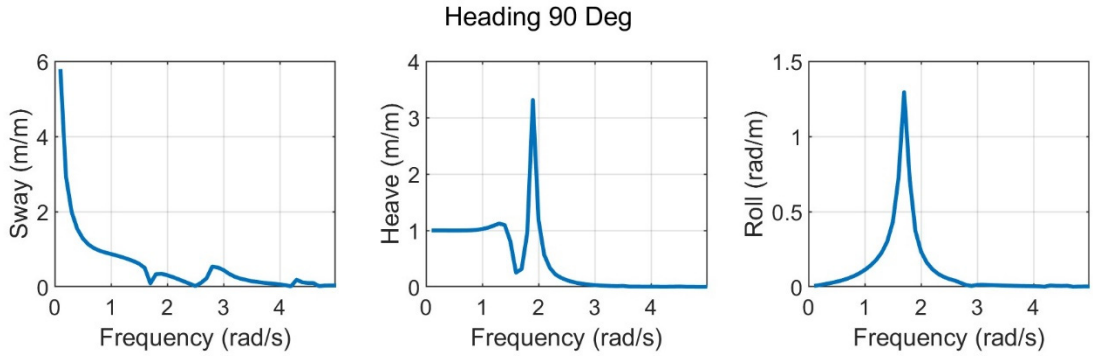

Figure 10. RAOs of catamaran in beam incident waves

4. Time domain simulation in random waves

Time-domain simulations were conducted on the three CTVs using an independent in-house computer program CHARM3D. The applied met-ocean properties are as discussed in the previous section. The time histories of random-wave elevations were generated and applied to the respective vessels to generate the corresponding motion time series. Then, the motion time series were converted to the corresponding motion spectra. Then, the time-series-regenerated x-RAOs were obtained from Eq. (2).

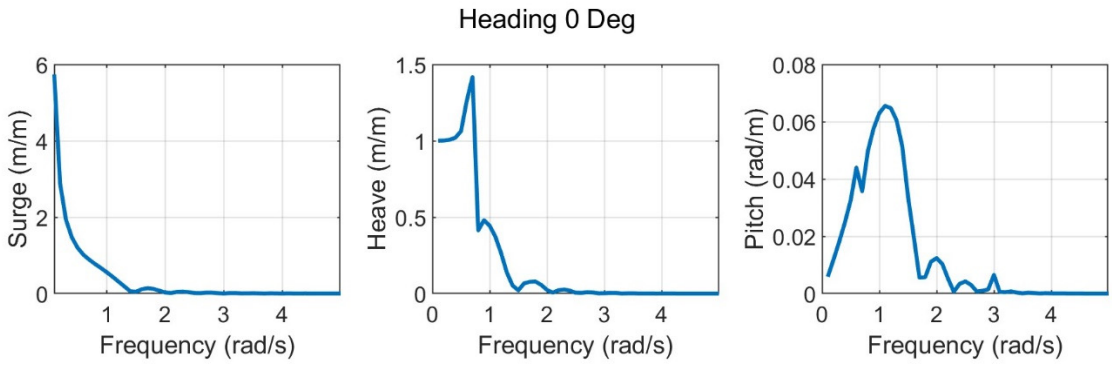

Figure 11. 6-DOF RAOs of SWATH in head incident waves

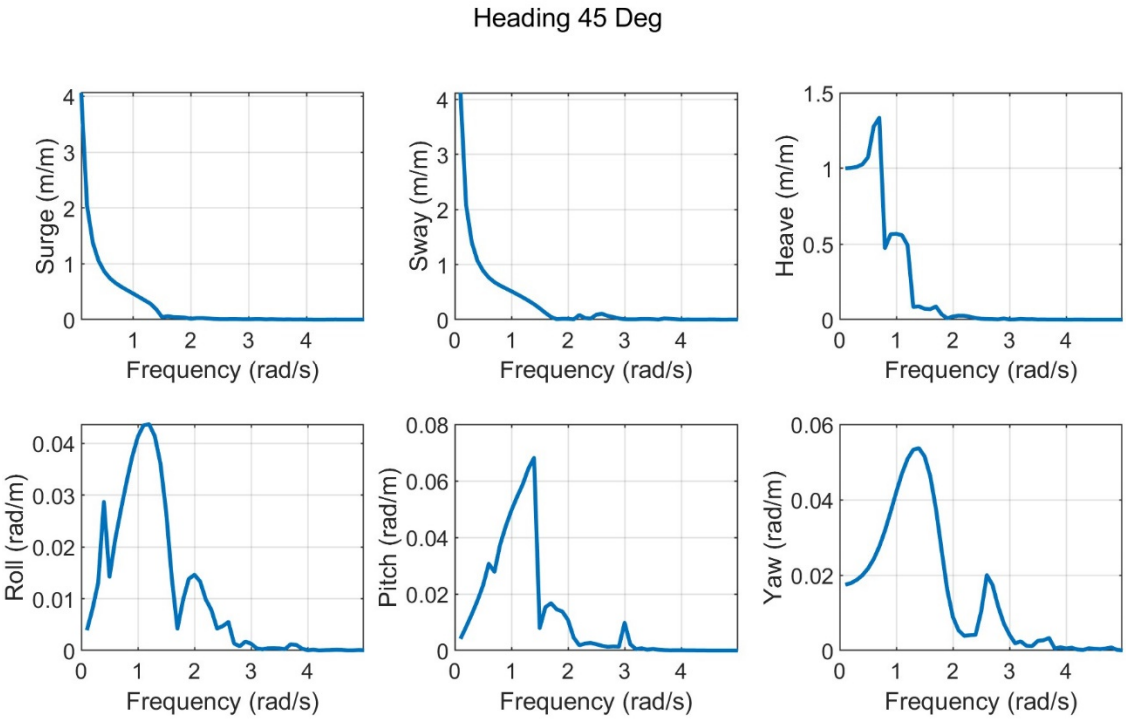

Figure 12. 6-DOF RAOs of SWATH in 45deg oblique incident waves

$$RAO(\omega) = \sqrt{\frac{S_{xx}(\omega)}{S_{\eta\eta}(\omega)}}, \tag{2}$$

The regenerated RAO can be obtained through the above equation only in the frequency range for which there is nontrivial incident wave amplitude. The resulting RAO comparisons between frequency-domain and time-domain calculations agree very well, which double-checked the correctness of both frequency-domain and time-domain calculations. In the time-domain

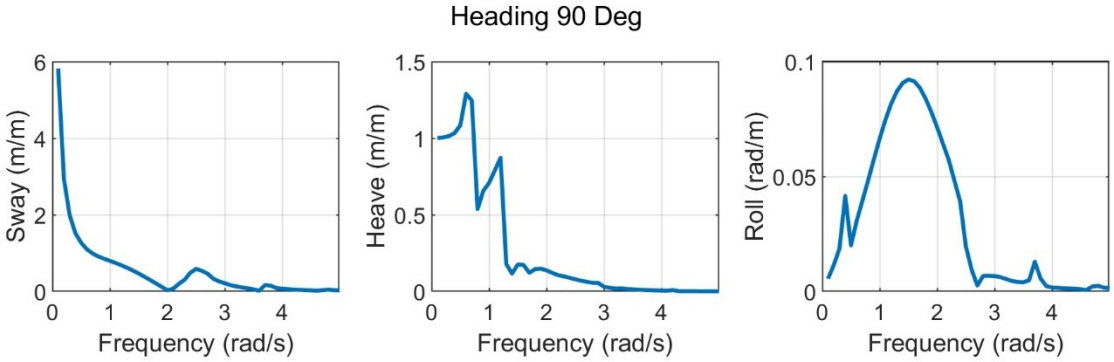

Figure 13. RAOs of SWATH in beam incident waves

Table 3. Selected sea states of 3 and 4, where H_s *is* significant wave height, T_p is peak wave period, and γ is spectral peakedness (enhancement or overshoot) parameter

	H_s (m)	T_p (s)	γ
Sea state 3	1.5	5.8 (1.08 rad/s)	3.3
Sea state 4	2.5	5.8	3.3

simulations of catamaran and SWATH, viscous drag forces are included through nonlinear (relative- velocity-squared) Morison equation for multiple Morison members, the effects of which are important to reduce the resonance-response peaks.

4.1 Input wave conditions

The mission of the present paper is to compare the seakeeping performances of the three vessels in the upper limits of sea state 3 and 4 to find the corresponding safety and operability of offshore crew transfer. So, the following typical sea state 3 and 4 are selected.

A 3-parameter (H_s, T_p, γ) JONSWAP wave amplitude spectrum was used as input wave spectrum and to generate the corresponding random wave time series. The input spectrum and wave-elevation time series are shown in Figs. 14 and 15. The lowest and highest cut-off frequencies, 0.7 and 2.0 rad/s, were used for the spectrum and the entire frequency range between them was divided by 100 component waves with non-uniform (randomly perturbated) interval so that signal repetition may not happen.

4.2 Safety of crew transfer

Transfer performance is typically illustrated with P-plots, showing operational limits for significant wave heights across different wave directions as shown in Fig. 16. Phillips et al. [12] also used P-plots as a practical method for presenting motion limits and transfer performance across wave directions and sea states, helping to bridge prediction data with real-world trials. The authors have also presented a methodology for assessing CTV operational availability based on vessel size, cost, and environmental conditions, highlighting that design decisions particularly regarding speed, thrust, and motion control directly impact commercial efficiency [13-15].

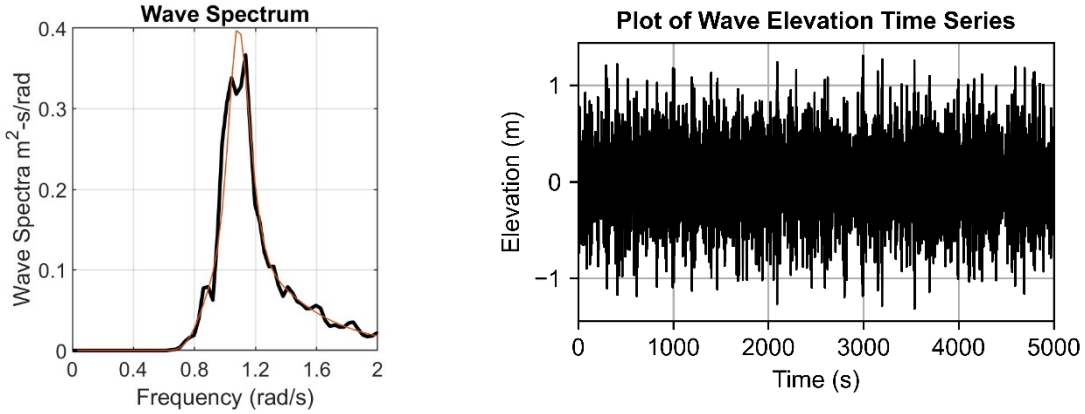

Figure 14. Input JONSWAP wave spectra and the corresponding time series of the selected sea state 3. The red curve in wave spectrum plot is the theoretical JONSWAP wave spectra and the black curve is regenerated JONSWAP wave spectra from time simulation

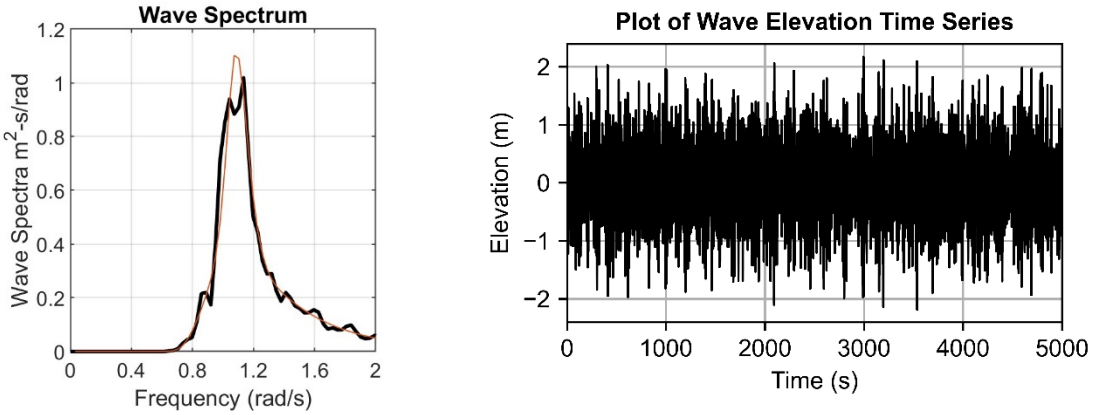

Figure 15. Input JONSWAP wave spectra and the corresponding time series of the selected sea state 4. The red curve in wave spectrum plot is the theoretical JONSWAP wave spectra and the black curve is regenerated JONSWAP wave spectra from time simulation

Seakeeping, also presented through P-plots, determines the vessel's ability to operate at higher transit speeds, extend operational windows, and increase wind farm accessibility.

Understanding these limitations is essential for optimizing vessel design, improving transfer reliability, and supporting the offshore wind sector's broader goals of efficiency and sustainability.

In summary, CTVs typically operate up to 1.5-2.0 m significant wave height depending on wave direction, beyond which safety is of concern. Acceptable acceleration rms thresholds are ~0.05 g vertical and ~0.04 g horizontal, with roll kept below ~3° for safe crew transfer. Of course, the criteria may differ depending on transfer methods.

4.3 Methodology of time-domain simulation

In time domain simulations, the motion time histories are commonly generated using Cummin's equation as follows [17, 18]

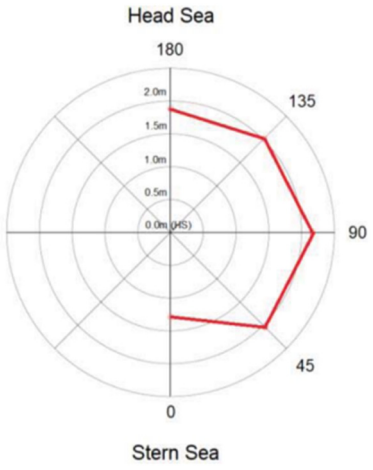

Figure 16. Example of P - plot showing CTV capability in variety of sea directions [16]

$$\left(\mathbf{M}+\mathbf{M}_{\mathbf{a},\infty}\right)\ddot{\xi}(t)=\mathbf{F}_{\mathbf{w1}}(t)+\mathbf{F}_{\mathbf{w2}}(t)+\mathbf{F}_{\mathbf{C}}(t)+\mathbf{F}_{\mathbf{restoring}}(t)+\mathbf{F}_{\mathbf{Drag}}(t)+\mathbf{F}_{\mathbf{M}}(t), \tag{3}$$

where $\mathbf{M}$, $\mathbf{M}_{\mathbf{a},\infty}$, $\mathbf{F}_{\mathbf{w1}}$, $\mathbf{F}_{\mathbf{w2}}$, $\mathbf{F}_{\mathbf{C}}$, $\mathbf{F}_{\mathbf{restoring}}$, $\mathbf{F}_{\mathbf{Drag}}$, and $\mathbf{F}_{\mathbf{M}}$ are mass matrix, added mass matrix at infinite frequency, 1st-order wave force, 2nd-order wave force, radiation damping force in the form of convolution integral, hydrostatic restoring force, viscous drag force, and other external force such as mooring or thruster forces. In the present case, no mooring or thruster forces are considered. $\ddot{\xi}(t)$ is the 6-DOF body acceleration. The frequency-dependent hydrodynamic coefficients – including added mass, radiation damping, and wave excitation forces – were obtained using the 3-D diffraction/radiation panel program WAMIT. The viscous drag force ($\mathbf{F}_{\mathbf{Drag}}$) is represented through the relative-velocity-based quadratic drag component of the Morison equation.

$$\mathbf{F}_{\mathbf{Drag}}=\frac{1}{2}\rho C_D A_p(\mathbf{u}-\dot{\xi})|\mathbf{u}-\dot{\xi}|. \tag{4}$$

where ρ, C_D, A_p, u, and $\dot{\xi}$ are the fluid density, the drag coefficient, the projected area for Morison structure elements, wave-induced fluid particle velocity, and the body velocity, respectively. In the case of monohull, the equivalent linear viscous roll damping was used instead of the Morison equation. In the case of catamaran and SWATH, the Morison equation was used to reflect viscous drag effects. The second-order wave force ($\mathbf{F}_{\mathbf{w2}}$) is not considered here since it plays an appreciable role only in the dynamics of moored platforms, which is not the case in the present study. In the beginning of time-domain simulation, all the wave forces were gradually applied from zero to actual values to minimize the unnecessary transient responses.

4.4 Results of time-domain simulations

In the following, time-domain simulation results are presented for heave and pitch in the head wave of sea state 3 and 4. The initial ramping time of 1500s was used to obtain meaningful steady-state signals during the next 3000s, from which motion spectra were calculated for the

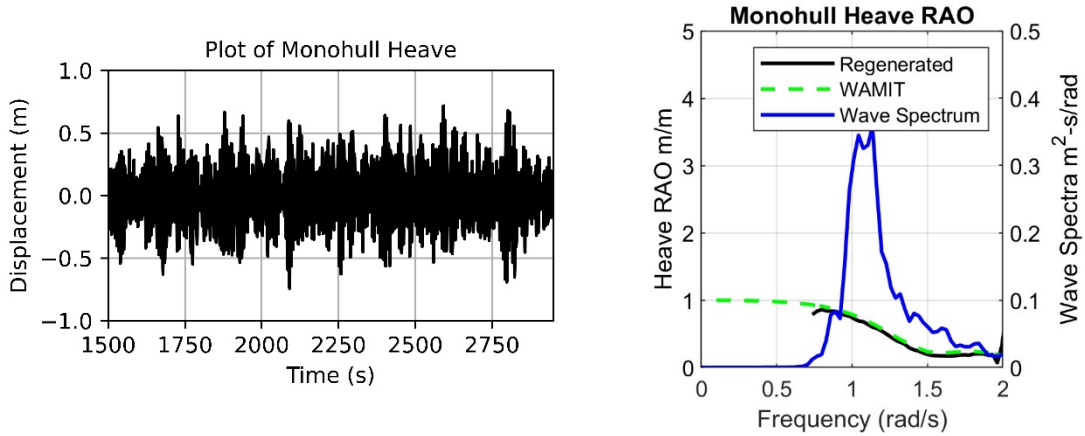

Figure 17. Heave time series, original (WAMIT) RAOs, and regenerated RAOs of monohull in the given wave spectrum of sea state 3

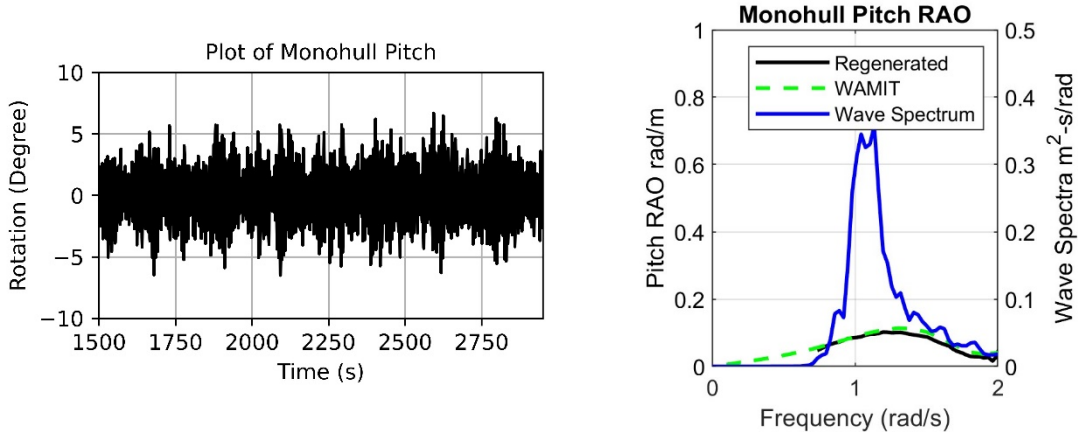

Figure 18. Pitch time series, original (WAMIT) RAOs, and regenerated RAOs of monohull in the given wave spectrum of sea state 3

regenerated RAOs. In the following, WAMIT means frequency-domain calculation by WAMIT program and 'Regenerated' means regenerated RAO using Eq. (2) based on the generated motion time series and spectra. In the frequency-domain vs. time-domain RAO comparisons, the incident wave spectrum is also given as a reference. In the case of regenerated RAO from motion time histories and Eq. (2), the results are meaningful within the range of nontrivial wave energy, so it is truncated at 0.7 rad/s.

4.4.1 Mono-hull case

The frequency-domain-calculated RAOs agree well with time-domain-calculated RAOs, which means both calculations were done correctly in a consistent manner. The typical heave range of monohull in sea state 3 and 4 are within $\pm$0.75 and $\pm$1.3. This means that monohull is operable in the head wave of sea state 3 but risky in sea state 4.

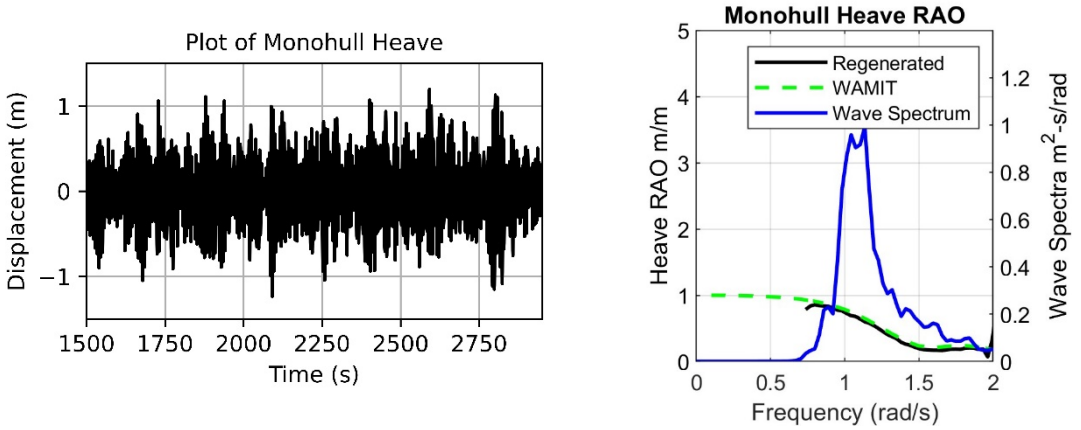

Figure 19. Heave time series, original (WAMIT) RAOs, and regenerated RAOs of monohull in the given wave spectrum of sea state 4

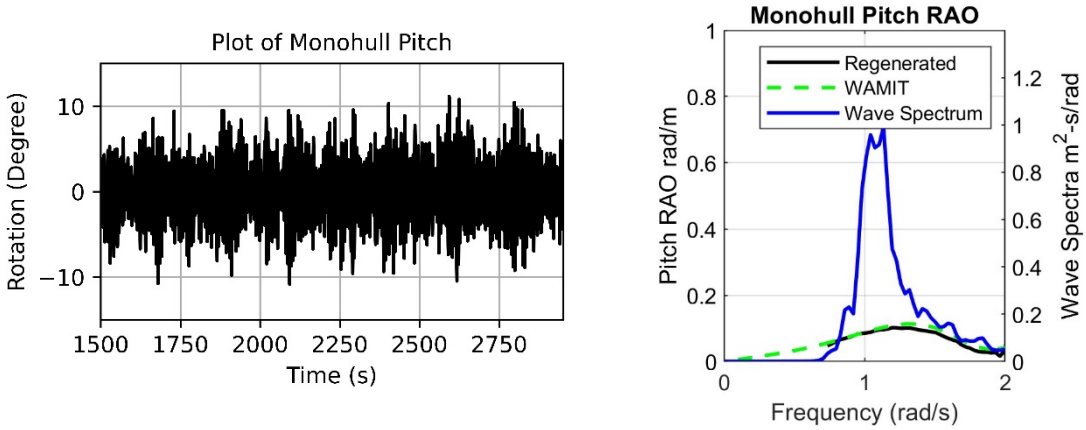

Figure 20. Pitch time series, original RAOs, and regenerated RAOs of monohull in the given wave spectrum of sea state 4

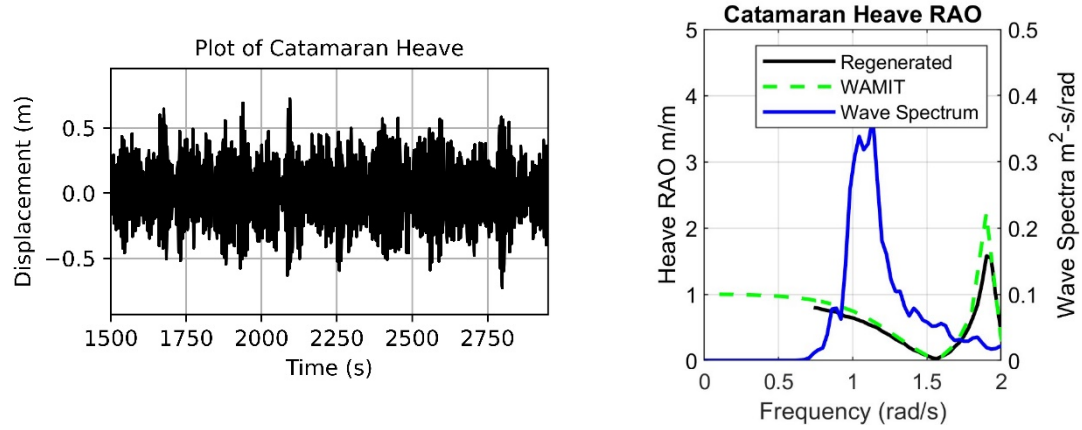

Figure 21. Heave time series, original (WAMIT) RAOs, and regenerated RAOs of catamaran in the given wave spectrum of sea state 3

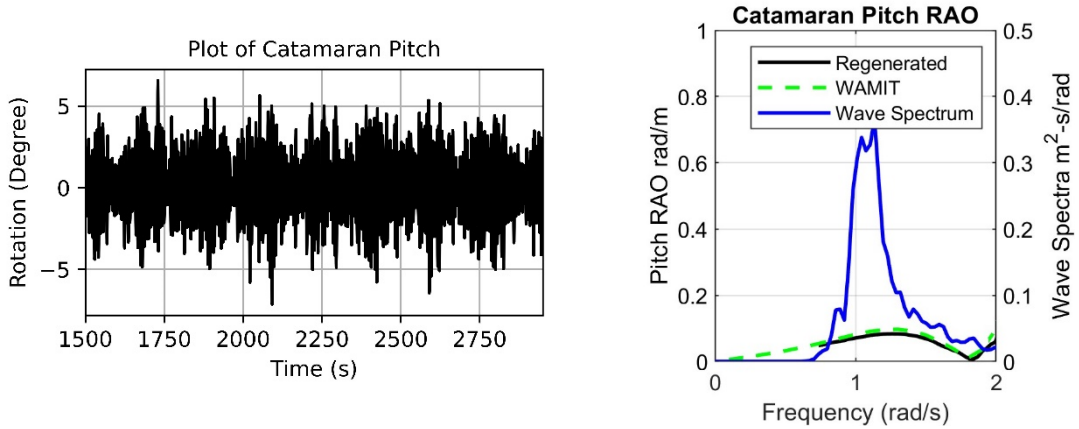

Figure 22. Pitch time series, original (WAMIT) RAOs, and regenerated RAOs of catamaran in the given wave spectrum of sea state 3

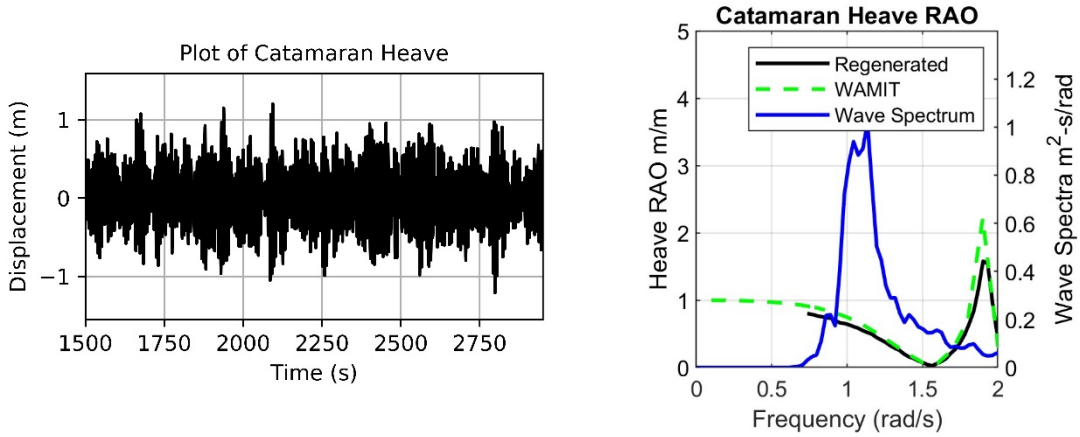

Figure 23. Heave time series, original (WAMIT) RAOs, and regenerated RAOs of catamaran in the given wave spectrum of sea state 4

4.4.2 Catamaran case

As pointed out earlier, Morison Plate Members are used here to capture the viscous drag of the fluid on twin vertical hulls (thickness=1.5 m, draft=2 m). Two (front and rear) Morison members are located along the longitudinal center line of each hull. At the center of each Morison member, the corresponding relative-velocity-based drag forces are calculated with respect to its instantaneous position. The drag coefficient for the Morison Plate Member was 2 in the normal direction. The respective time series exclude initial transient part as explained earlier.

Again, the frequency-domain calculations agree well with time-domain calculations. The overall trends of heave and pitch motion time series of catamaran are similar (with slightly less amplitudes) to those of monohull in the given sea state 3 and 4. The heave resonance peaks (around 1.9 rad/s) are reduced after including viscous effects in the time domain.

The maximum heave-pitch motion range is very similar to that of monohull. The catamaran would have reduced heave-pitch motions in shorter-period waves (around 1.1~1.5 rad/s) but they

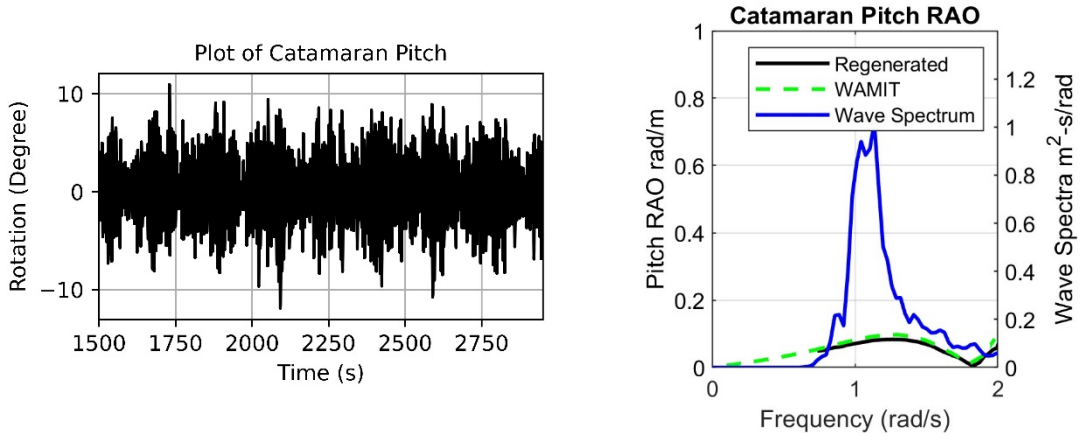

Figure 24. Pitch time series, original (WAMIT) RAOs, and regenerated RAOs of catamaran in the given wave spectrum of sea state 4

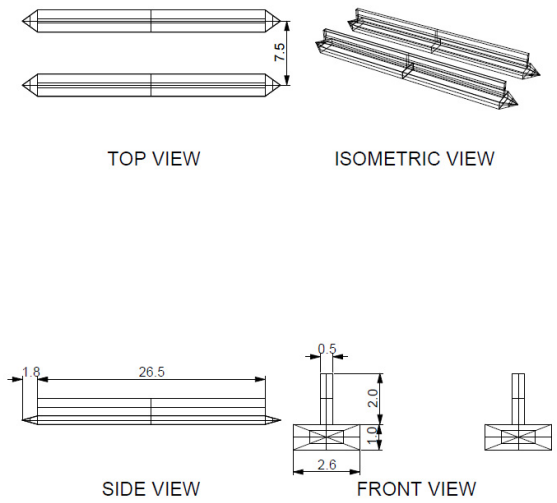

Figure 25. Geometry of the present SWATH vessel (All units in meter)

can increase in shorter waves near 1.9rad/s compared to monohull. The above result shows that the catamaran motion characteristics are slightly better than those of monohull but still cannot be used safely in sea state 4. Whereas, the next section will show that SWATH can be used in sea state 4.

4.4.3 SWATH case

SWATH typically consists of thin vertical wall connected by bottom circular pontoons. In this paper, we used thin horizontal plate for the bottom pontoon to minimize the navigation resistance while maximizing heave added mass and viscous damping. The hull geometry is invented to achieve the targeted displacement while lowering its heave natural frequency far below the typical peak wave frequencies of sea states 3 and 4, which is possible through smaller waterplane area and increased heave-pitch-roll added mass. We used all straight hull surfaces to minimize the cost of

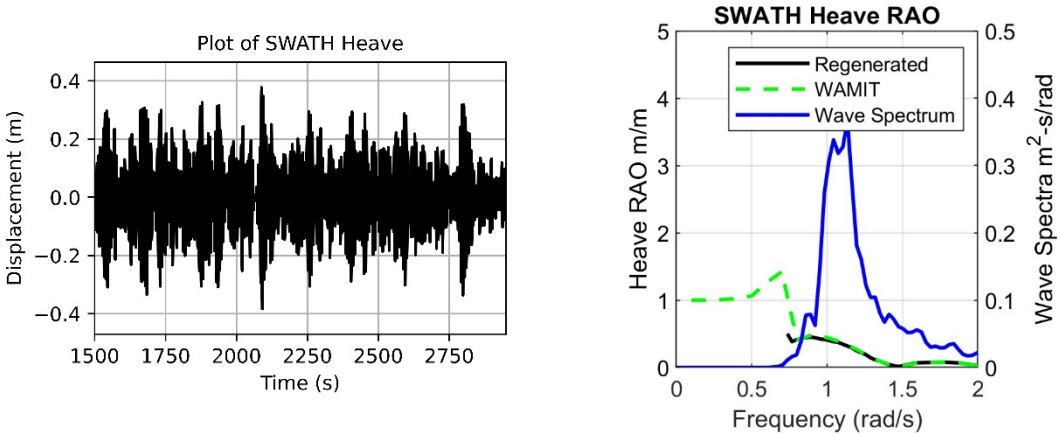

Figure 26. Heave time series, original (WAMIT) RAOs, and regenerated RAOs of SWATH in the given wave spectrum of sea state 3

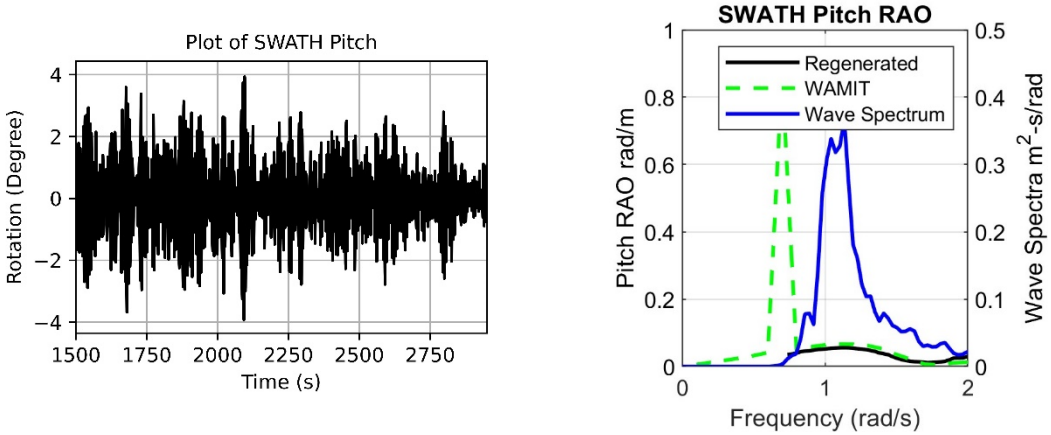

Figure 27. Pitch time series, original (WAMIT) RAOs, and regenerated RAOs of SWATH in the given wave spectrum of sea state 3

hull construction while satisfying the targeted performance. With the given hull form, heave, pitch, and roll natural frequencies are lower than 0.65 rad/s and the viscous damping from the flat pontoon is significantly increased to reduce resonance peaks.

As for SWATH, Morison plate members are used to capture the viscous drag of the fluid. In this case, two (front and rear) vertical Morison members were used for each thin vertical hull with $C_d = 2$ in normal direction. Also, two (front and rear) horizontal Morison members were used for each bottom pontoon with $C_d = 4$ in heave direction [19-21].

The simulated heave and pitch motions of SWATH for the same sea state 4 are in the range within $\pm$0.7 m and $\pm$7degrees, which is much smaller than those of monohull and catamaran. Again, the time-domain-regenerated heave and pitch RAOs agree well with the original frequency-domain WAMIT RAOs.

The heave-pitch ranges shown in SWATH's time series are less than half of the corresponding heave-pitch ranges of catamaran and monohull, which well demonstrate higher performance of

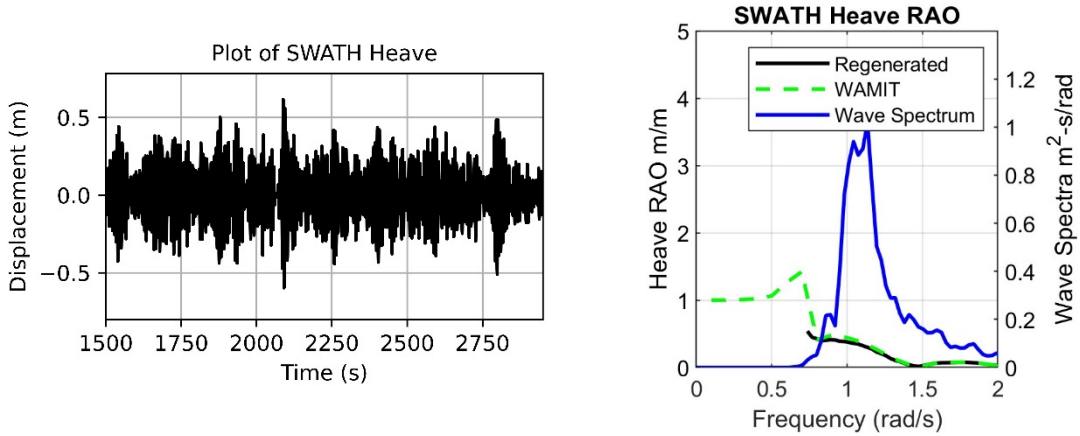

Figure 28. Heave time series, original (WAMIT) RAOs, and regenerated RAOs of SWATH in the given wave spectrum of sea state 4

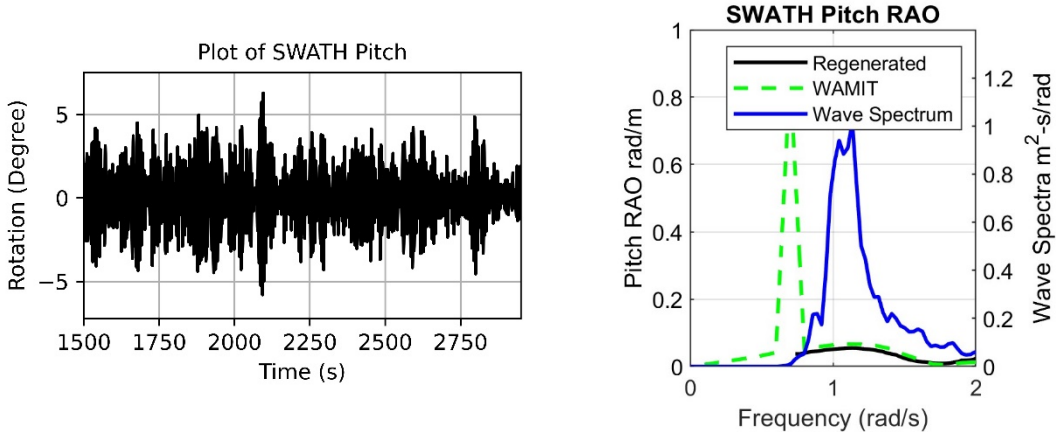

Figure 29. Pitch time series, original (WAMIT) RAOs, and regenerated RAOs of SWATH in the given wave spectrum of sea state 4

SWATH vessel in the operational sea state up to 4. This shows that SWATH can be a high-performance hull form to significantly expand the operable window of sea states up to high sea state 4.

5. Two-body cases

In the previous sections, the seakeeping performances of the 3 CTVs were compared. In this section, the change of catamaran's seakeeping performance when operating behind 10 m-diameter 15 MW monopile turbine is analyzed by using 2-body hydrodynamics simulation program, multibody WAMIT in the frequency domain and the corresponding multi-body time-domain simulation program CHARM3D.

The monopile is a fixed body, so only diffraction analysis is needed for it. As for the catamaran, both diffraction and 6DOF radiation in the vicinity of the monopile need to be run. It is assumed

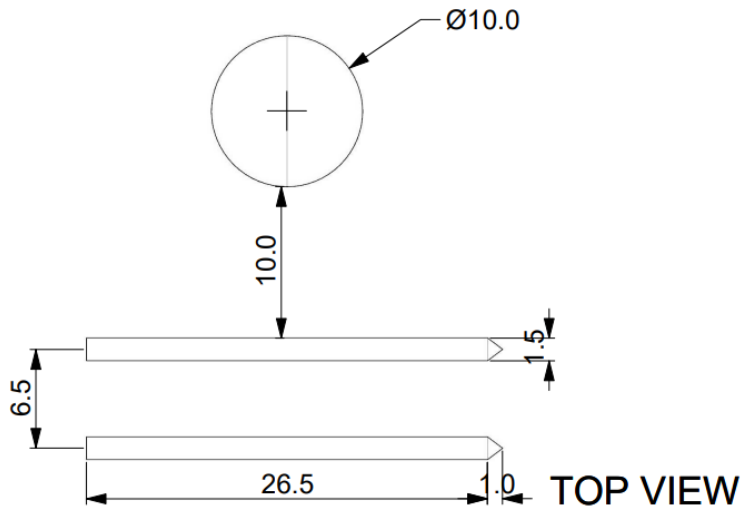

Figure 30. Arrangement of two-body interaction example for gangway crew transfer i.e. catamaran behind 10 m-diameter monopile (top view) (All units in meter)

Table 4. Sea states 3 and 4 considered for 2-body interaction case

	H_s (m)	T_p (sec)	γ
Sea state 3-II	1.4	4.5 (1.4 rad/s)	3.3
Sea state 4 (same as before)	2.5	5.8 (1.08 rad/s)	3.3

that the catamaran is positioned 10 m behind the monopile in beam-wave position and the corresponding safety of gangway transfer is considered. The set-up is shown in Fig. 30. The 2-body hydrodynamic coefficients including their interaction effects were calculated in the frequency domain by using multi-body WAMIT program. Then, the ensuing time-domain simulations were conducted by using in-house CHARM3D-Multibody program [22, 23]. For the given set-up, the catamaran-alone and catamaran-behind-monopile cases were systematically compared in sea state 3 and 4 to identify the resulting hydrodynamic interaction effects, which is followed by the same time-domain simulations of monohull and SWATH in sea state 4.

For this 2-body case, the H_s and T_p of sea state 3-II are slightly altered compared to the previous sea state 3-I. The sea state 4 has the same H_s, T_p, and γ as the previous case with different random-phase seed.

First, the sway-heave-roll RAOs of catamaran for the two cases is shown in Fig. 32, which is calculated by frequency-domain multi-body WAMIT. At 1.1 rad/s (peak of sea state 4), the reduction of catamaran heave behind the monopile can be noticed while there is little difference in sway and roll. At 1.4 rad/s (peak of sea state 3-II), the reduction of catamaran sway behind the monopile can be noticed while there is little difference in roll. In this case, the heave can slightly be increased as a result of the 2-body interaction.

Figs. 33 and 34 show the corresponding time-domain simulations of catamaran alone and those behind monopile in the beam wave of sea state 3-II. In the time-domain simulations, Morison drag forces and second-order wave forces are not included for convenience since they cause continuous

(a) (b)

Figure 31. Top view (a) and side view and (b) of panels of catamaran with monopile

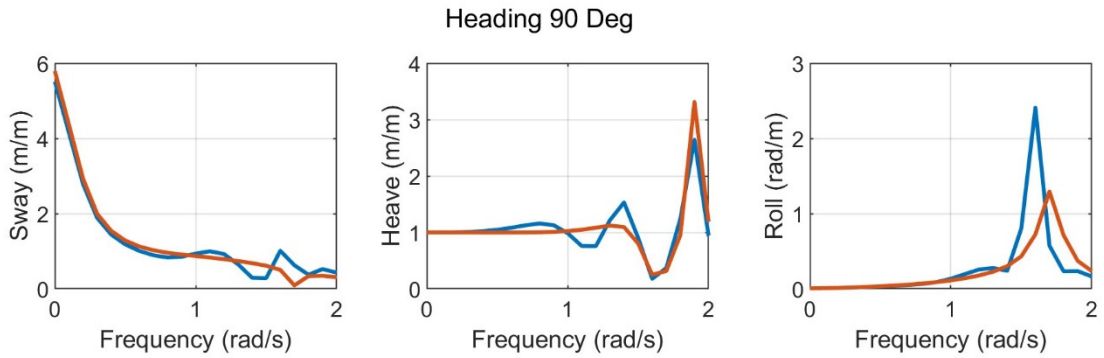

Figure 32. Catamaran sway-heave-roll RAOs in beam wave from 2-body WAMIT results compared to catamaran-alone case. Blue curve is Catamaran with Monopile. Orange curve is Catamaran only

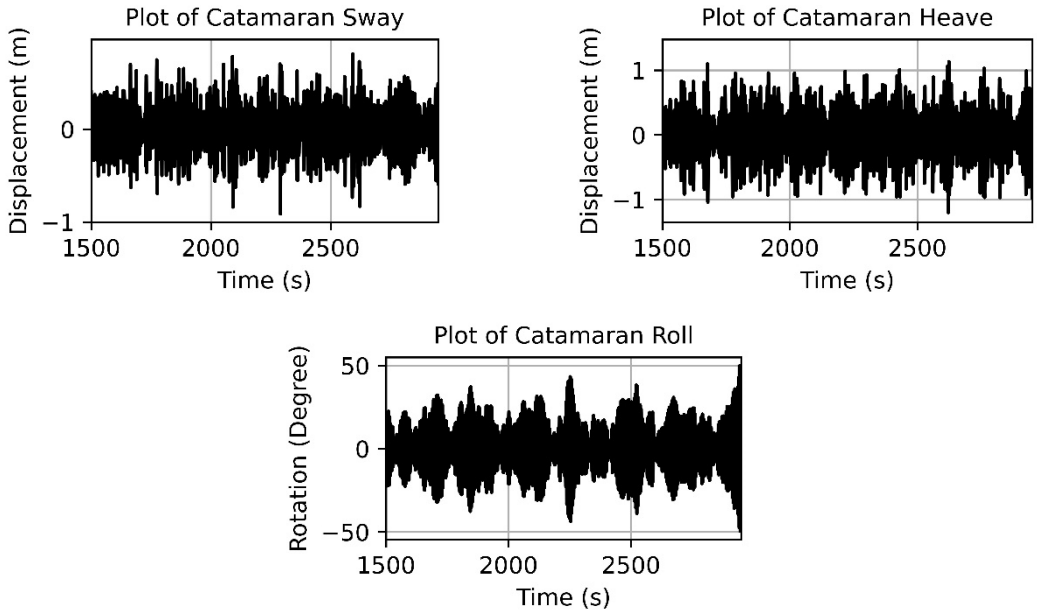

Figure 33. 3-DOF motion time series for catamaran only in beam wave of sea state 3-II

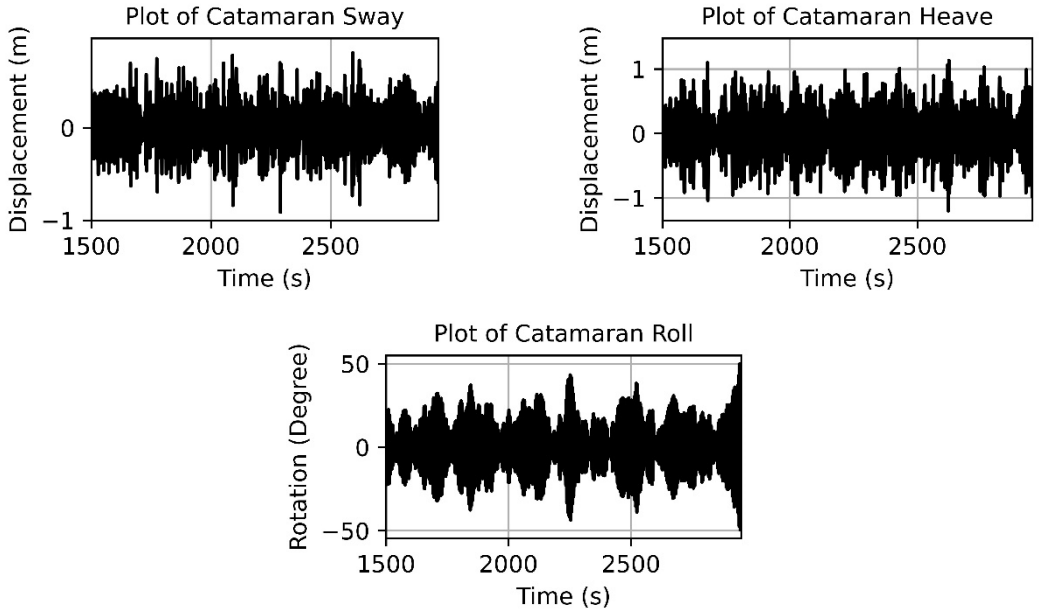

Figure 34. 3-DOF motion time series for catamaran behind monopile in beam wave of sea state 3-II

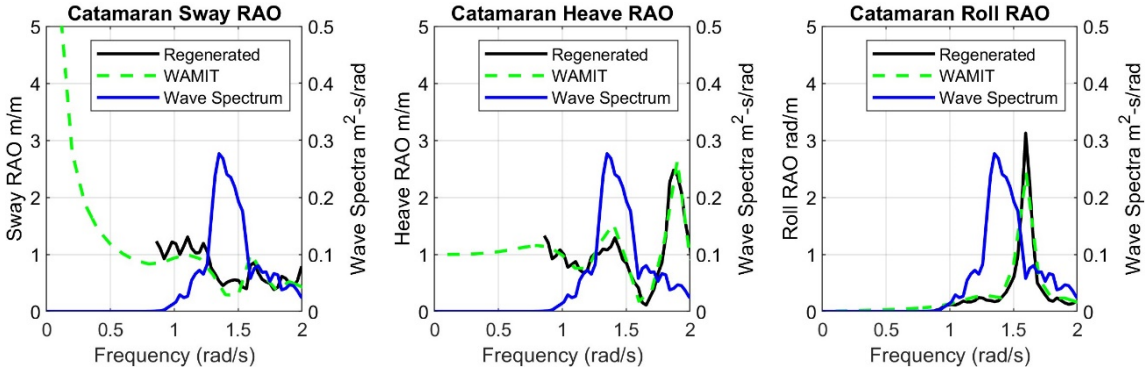

Figure 35. 3-DOF motion RAOs for catamaran behind monopile; frequency domain results by WAMIT and regenerated RAOs from motion time series in sea state 3-II

sway drift motions. In particular, the roll motion amplitudes are to be much smaller than the given results if viscous drag forces are included due to the reduction of resonance peak. From the simulated results, it is shown that at sea state 3-II (peak wave frequency near 1.4 rad/s), the shield effects by the monopile is small. From the time-domain simulation results of the 2-body case, the catamaran RAOs can be reconstructed as in Fig. 35. Both frequency and time-domain 2-body results show consistent results.

In Figs. 36-38, the same sets of results for sea state 4 are presented. In this case, since the peak wave frequency is moved to 1.1rad/s, slight heave reduction can be seen as a result of shielding effect behind monopile. Again, the 2-body time-domain simulation results agree well with the 2-body frequency-domain counter parts.

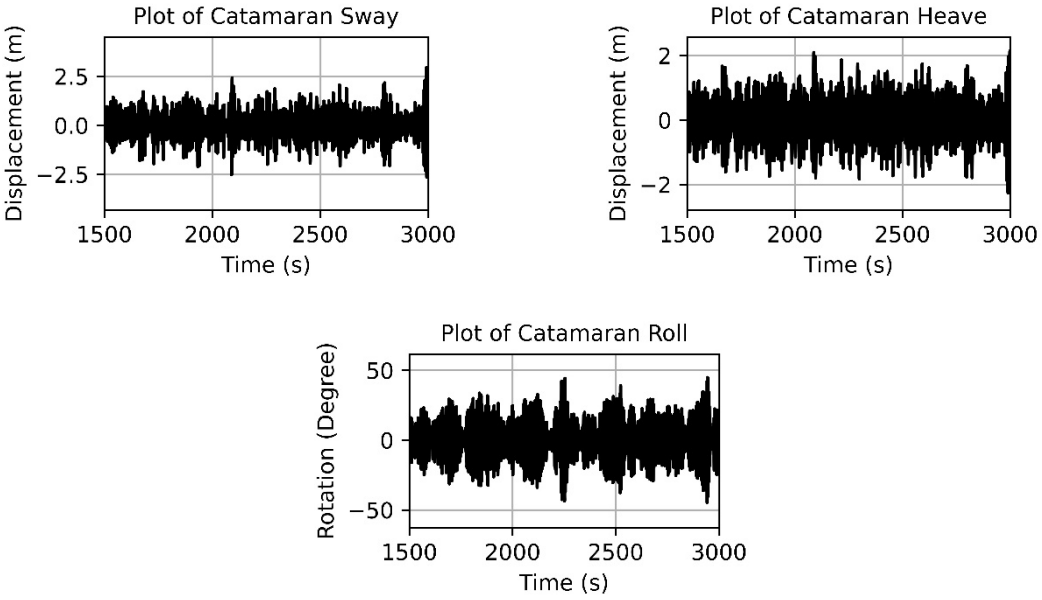

Figure 36. 3-DOF motion time series for catamaran only in beam wave of sea state 4

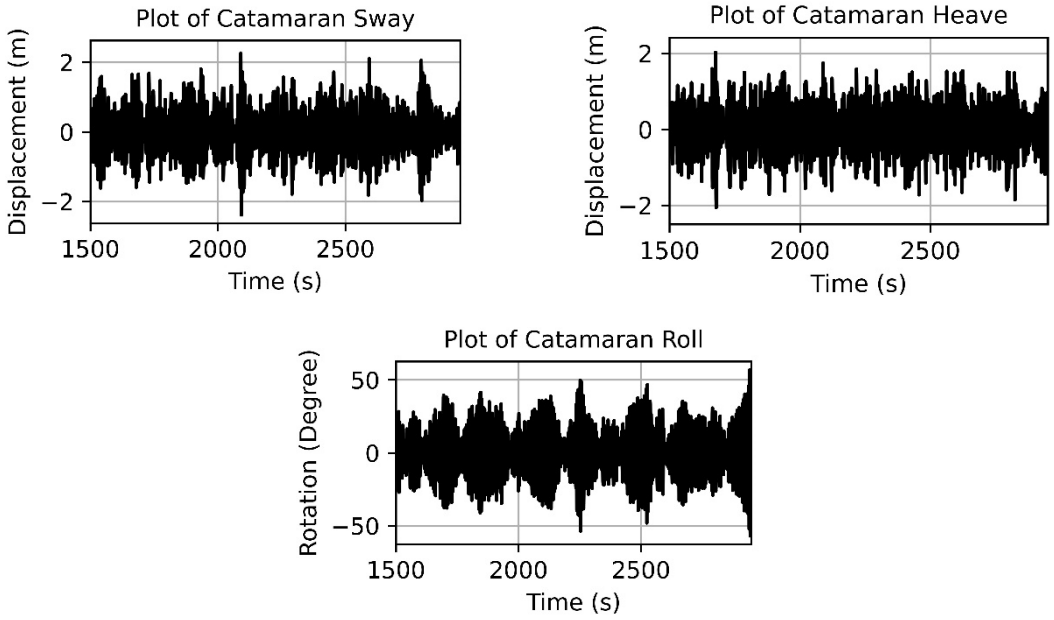

Figure 37. 3-DOF motion time series for catamaran behind monopile in beam wave of sea state 4

Next, 2-body interactions of monohull are considered. First, the sway-heave-roll RAOs of monohull corresponding to Fig. 32 are presented.

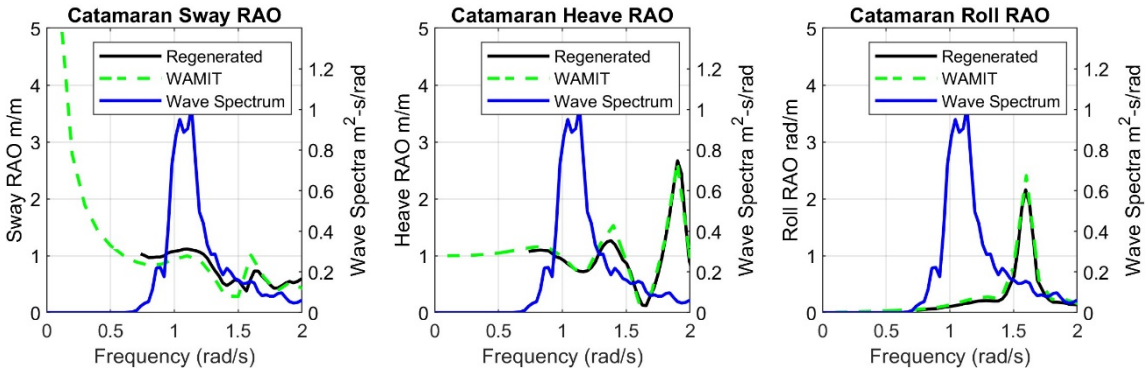

Figure 38. 3-DOF motion RAOs for catamaran behind monopile; frequency domain results by WAMIT and regenerated RAOs from motion time series in sea state 4

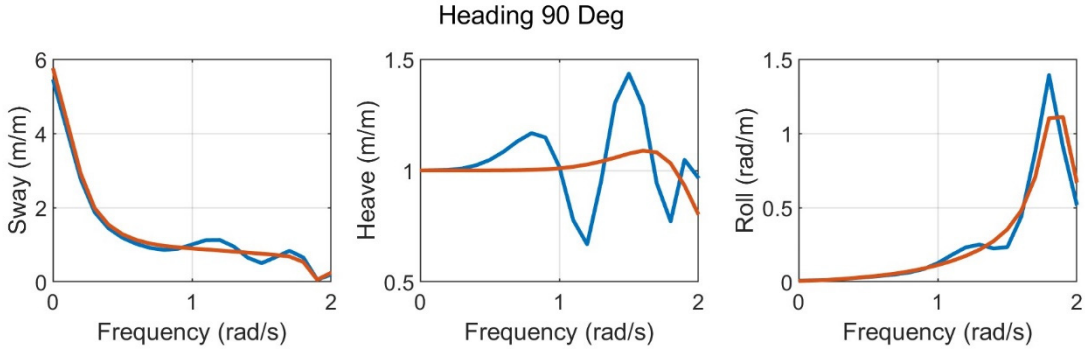

Figure 39. Monohull sway-heave-roll RAOs in beam wave from 2-body WAMIT results compared to Monohull-alone case. Blue curve is Monohull with Monopile. Orange curve is Monohull only

Fig. 40 shows the sway-heave-roll time histories of the monohull behind the monopile in the sea state 4. Fig. 41 shows the corresponding regenerated RAOs from the motion time series compared to the frequency-domain 2-body results. They agree very well. It is seen that their motion characteristics and trends are very similar to those of catamaran.

Figs. 43 and 44 show the sway-heave-roll time histories and similar RAO comparisons of the SWATH behind the monopile in sea state 4. The effects of 2-body interaction of SWATH are much smaller than those of catamaran and monohull. The maximum and overall heave and roll amplitudes of SWATH are significantly reduced compared to those of catamaran and monohull. Considering the strict guideline of maximum allowable movement of $\pm$0.5 m for sway and $\pm$1 m for heave and $\pm$30degrees in roll, the SWATH is highly operable even in the upper sea state 4, which is consistent with the field observation and recommended practice in wind-energy industry. Further reduction of the 3DOF motions after including Morison drag effects is also expected, which makes SWATH highly preferable to catamaran and monohull from the perspective of expanding operational window up to the high sea state 4.

Judging from the above 2-body simulation results, the following remarks are made. In general, sway-heave-roll motions of CTVs only in beam waves are slightly larger than those behind 10 m diameter monopile due to shielding effects. However, the shielding effects are small and may

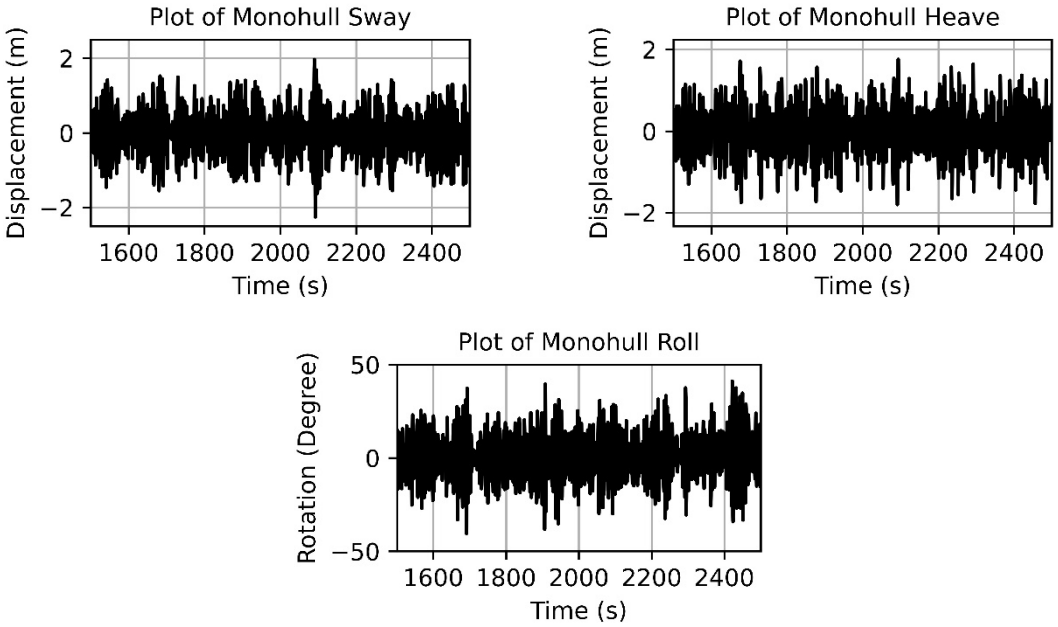

Figure 40. 3-DOF motion time series of monohull behind monopile in beam wave of sea state 4

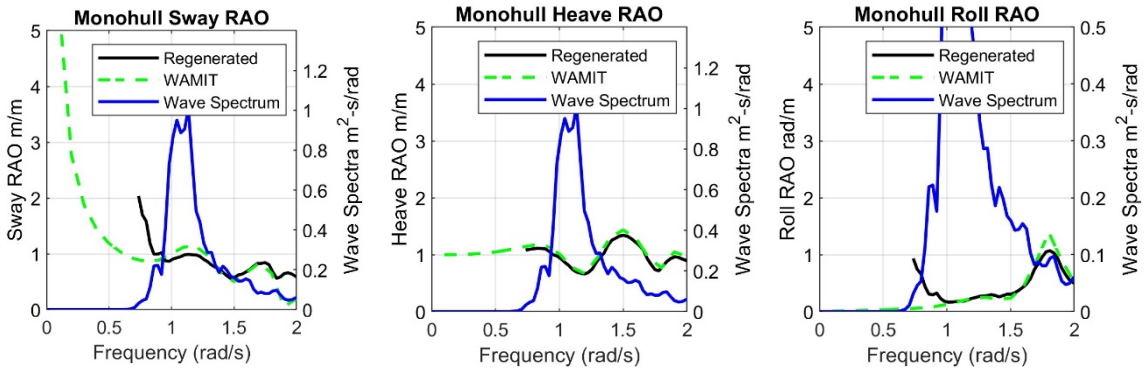

Figure 41. 3-DOF motion RAOs for monohull behind monopile; frequency domain results by WAMIT and regenerated RAOs from motion time series in sea state 4

Table 5 Comparison of motion performance behind monopile among 3 CTVs in sea-state 4

	Sway rms	Sway acceleration rms	Heave rms	Heave acceleration rms	Roll rms
Catamaran	0.64 m	0.91 m/s^2	0.66 m	1.17 m/s^2	16.9 deg
Monohull	0.65 m	0.86 m/s^2	0.58 m	1.05 m/s^2	13.87 deg
SWATH	0.53 m	0.79 m/s^2	0.37 m	0.44 m/s^2	2.43 deg

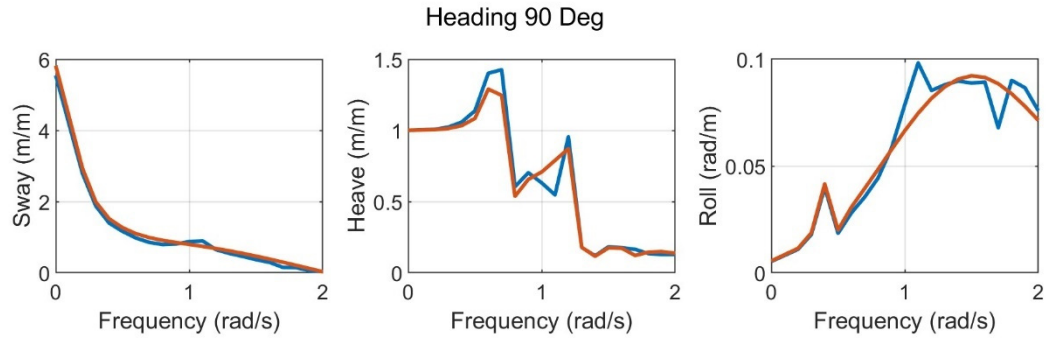

Figure 42. SWATH sway-heave-roll RAOs in beam wave from 2-body WAMIT results compared to SWATH-alone case. Blue curve is SWATH with Monopile. Orange curve is SWATH only

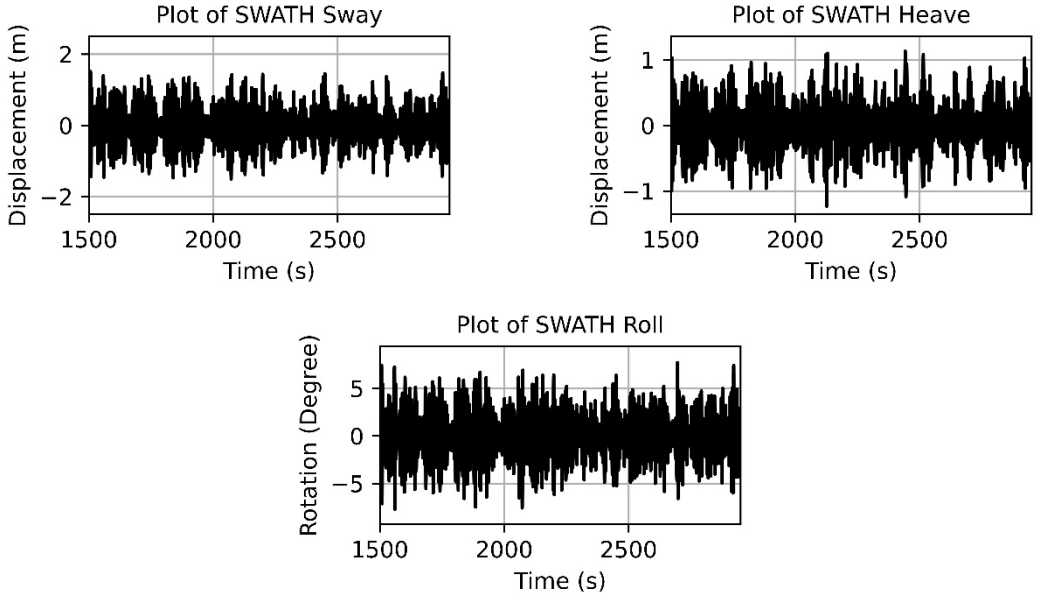

Figure 43. 3-DOF motion time series for SWATH behind monopile in beam wave of sea state 4

depend on the motion characteristics of vessels and incoming waves. Therefore, in case of 10 m diameter monopile, the single-body-motion case can be considered as a reasonable first-cut approach in assessing the safety of crew transfer.

As can be demonstrated in Table , the seakeeping performance of SWATH with monopile in sea state 4 is significantly better than those of catamaran and monohull. In particular, the reduction of SWATH's heave and roll compared to monohull and catamaran is significant.

6. Conclusions

To compare the seakeeping performances of monohull, catamaran, and SWATH of similar displacement and principal dimensions, three respectively generic CTVs are designed by authors

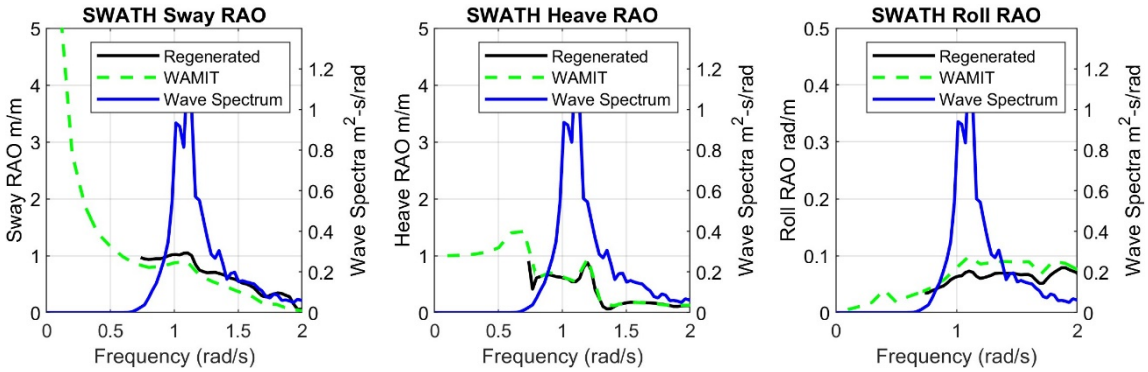

Figure 44. 3-DOF motion RAOs for SWATH behind monopile; frequency domain results by WAMIT and regenerated RAOs from motion time series in sea state 4

for fair comparison. The RAOs were calculated from potential theory and BEM in the frequency domain and they were systematically compared with the regenerated RAOs from time-domain simulations and they showed good agreements.

When comparing seakeeping performances in sea states 3 and 4 among the three generic CTVs with similar displaced mass and principal dimensions, catamaran and monohull performed similarly and SWATH performed the best. In particular, the newly invented SWATH with flat pontoons demonstrated highly favorable seakeeping performances with potentially minimal resistance during navigation.

Our SWATH's 6DOF motion amplitudes are about half of those of catamaran and monohull in sea state 3 and 4 regardless of wave directions. Therefore, SWATH can be operated up to high sea state 4 while monohull & catamaran can be used up to sea state 3. SWATH motions are reduced since their heave-roll-pitch natural frequencies are much lower than the spectral frequency range of sea state 3 and 4. The SWATH's increased added mass and reduced waterplane area contributed to its preferable seakeeping performance. Its roll restoring moment is reduced but it can be compensated by favorable location of center of gravity. As a result, SWATH can significantly expand the operational window up to high sea state 4, and is particularly useful for long-distance missions for wind farms.

Two-body (monohull, catamaran, and SWATH behind 10m-diameter monopile in beam waves) hydrodynamic interactions showed modest shielding effects but it depends on CTV motion characteristics and shapes of incident wave spectra. In the two-body case, SWATH demonstrated significantly better motion performance in sea state 4 compared to monohull and catamaran.

Similar research for CTVs and large floating wind turbines [18] are needed (with/without heave compensated crew transfer mechanisms), for which the features of 2-body hydrodynamic interactions are to be more complex.

Acknowledgements

This research was sponsored by the Ocean Energy Safety Institute Consortium (OESIC) through a grant from the U.S. Department of the Interior, Bureau of Safety and Environmental Enforcement (BSEE), and the U.S. Department of Energy (DOE) and was accomplished under

Agreement Number E21AC00000. The views and conclusions contained in this document are those of the authors and should not be interpreted as representing the opinions or policies of the U.S. Government. Mention of trade names or commercial products does not constitute their endorsement by the U.S. Government.

References

1. Wu, M. (2014). Numerical analysis of docking operation between service vessels and offshore wind turbines. Ocean Engineering, 91, 379-388. https://doi.org/10.1016/j.oceaneng.2014.09.027.
2. Thiagarajan, K., Lekkalaa, M.R., Kim, M.H., Wang, S. (2026). Crew transfer CTV to offshore wind turbines - a state-of-the-art review. Ocean Engineering, Art no. 124537.
3. Otsubo, K. (2023). Stick/slip phenomenon of a crew transfer vessel pushing its bow against an offshore wind tower during a transfer operation. International Journal of Offshore and Polar Engineering, 33(4), 409-419. https://doi.org/10.17736/ijope.2023.jc898.
4. Otsubo, K. and Ishida, K. (2024). Comparison of stick/slip phenomena at transfer points between different hull-type CTVs. Proceedings of the 34th International Ocean and Polar Engineering Conference.
5. Otsubo, K., Ishida, K. (2025). Comparative investigation of the transfer performance between catamaran-, monohull- and SWATH-type CTVs. Proceedings of the 35th International Ocean and Polar Engineering Conference.
6. Guanche, R., Martini, M., Jurado, A., Losada, I.J. (2016). Walk-to-work accessibility assessment for floating offshore wind turbines. Ocean Engineering, 116, 216-225. https://doi.org/10.1016/j.oceaneng.2016.03.013.
7. Gutsch, M., Ludvigsen, H., Jagite, G., Steen, S., Sprenger, F. (2025). Relative motion RAOs for efficient simulation of marine operations for floating wind farms. Applied Ocean Research, 161, 104634. https://doi.org/10.1016/j.apor.2025.104634.
8. Lee, C.H. (1995). WAMIT theory manual. Massachusettes Institute of Terchnology, Cambridge, MA.
9. Kim, M.H., Ran, Z., Zheng, W. (2001). Hull/mooring coupled dynamic analysis of a truss spar in time domain. International Journal of Offshore and Polar Engineering, 11(1), 42-54.
10. Barthelemy, L. (2023). O&M of crew transfer vessels against floating wind turbines -- modelling the water run-up effect during personnel transfer in waves with short periods.
11. Chung, J.S., Kim, M.H. (1995). Added mass and damping on an oscillating surface-piercing column with a horizontal cylinder: square cross sections. International Journal of Offshore and Polar Engineering, 5(3).
12. Phillips, S., Armstrong, C. (2015). Crew transfer vessel performance evaluation.
13. Guide for Certification of Offshore Access Gangways (2016). ABS, Spring, TX.
14. Guidance Notes on Risk Assessment Applications for the Marine and Offshore Industries (2020). ABS, Spring, TX.
15. Certification of Offshore Access Systems (2016). NI 629, BV.
16. Chivilo, F., Page, A. (2022). Design evolution of CTV vessels. Proceeings of the IOP Conference Series: Earth and Environmental Science, 1073(1), 012008. https://doi.org/10.1088/1755-1315/1073/1/012008.
17. Orcina (2025). OrcaFlex user manual. Orcina. https://www.orcina.com/webhelp/OrcaFlex/Redirector.htm?Whatwasnewinpreviousversions.htm#11.5.
18. Lee, I., Li, D., Fu, S., Yi, C., Kim, M., Ran, A., Liu, T. (2026). Experimental and numerical investigation on the dynamic response of a 15 MW semisubmersible floating offshore wind turbine including 1-mooring line failure scenario. Ocean Engineering, 343, 122980. https://doi.org/10.1016/j.oceaneng.2025.122980.

19. Kim,H., Lee, I., Kim, M.H., Jang, H., Koo, B. (2025). Development of variable-fidelity FOWT digital twins in extreme sea environments: Part I-mid-fidelity analysis. Ocean Systems Engineering, 15(1), 23-42. https://doi.org/10.12989/ose.2025.15.1.023.
20. Jang, H.C., Jang, H.K., Kim, M.H., Koo, B. (2025). Development of variable-fidelity FOWT digital twins in extreme sea environments: part II – high-fidelity CFD analysis. Ocean Systems Engineering, 15(1), 43-62. https://doi.org/10.12989/ose.2025.15.1.043.
21. Jang, H.K., Park, S., Kim, M.H., Kim, K.H., Hong, K. (2019). Effects of heave plates on the global performance of a multi-unit floating offshore wind turbine. Renewable Energy, 134, 526-537, https://doi.org/10.1016/j.renene.2018.11.033.
22. Koo, B.J., Kim, M.H. (2005). Hydrodynamic interactions and relative motions of two floating platforms with mooring lines in side-by-side offloading operation. Applied Ocean Research, 27(6), 292-310. https://doi.org/10.1016/j.apor.2006.02.001.
23. Zainuddin, M., Kim, M., Jin, C., Bhat, S. (2023). Fully coupled multi-hull/mooring/riser/hawser time domain simulation of TLP-TAD system with MR damper. Ocean Systems Engineering, 13(4), 401-421. https://doi.org/10.12989/ose.2023.13.4.401.